

Task Aware Dreamer for Task Generalization in Reinforcement Learning

Chengyang Ying, Zhongkai Hao, Xinning Zhou, Hang Su, Songming Liu, Dong Yan, Jun Zhu

Department of Computer Science & Technology, Institute for AI, BNRist Center,
Tsinghua-Bosch Joint ML Center, THBI Lab, Tsinghua University;

Abstract

A long-standing goal of reinforcement learning is to acquire agents that can learn on training tasks and generalize well on unseen tasks that may share a similar dynamic but with different reward functions. The ability to generalize across tasks is important as it determines an agent’s adaptability to real-world scenarios where reward mechanisms might vary. In this work, we first show that training a general world model can utilize similar structures in these tasks and help train more generalizable agents. Extending world models into the task generalization setting, we introduce a novel method named Task Aware Dreamer (TAD), which integrates reward-informed features to identify consistent latent characteristics across tasks. Within TAD, we compute the variational lower bound of sample data log-likelihood, which introduces a new term designed to differentiate tasks using their states, as the optimization objective of our reward-informed world models. To demonstrate the advantages of the reward-informed policy in TAD, we introduce a new metric called Task Distribution Relevance (TDR) which quantitatively measures the relevance of different tasks. For tasks exhibiting a high TDR, i.e., the tasks differ significantly, we illustrate that Markovian policies struggle to distinguish them, thus it is necessary to utilize reward-informed policies in TAD. Extensive experiments in both image-based and state-based tasks show that TAD can significantly improve the performance of handling different tasks simultaneously, especially for those with high TDR, and display a strong generalization ability to unseen tasks.

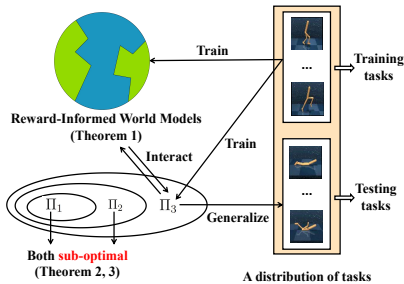
1 Introduction

Deep Reinforcement Learning (DRL) has demonstrated significant advancements in diverse fields [Mnih *et al.*, 2016; Hafner *et al.*, 2019a], and a key factor in these accomplishments is an agent’s proficiency in assimilating lessons from dedicated training tasks. However, when the objective transitions from optimizing performance in specific tasks to achieving broad generalization across related tasks, new challenges

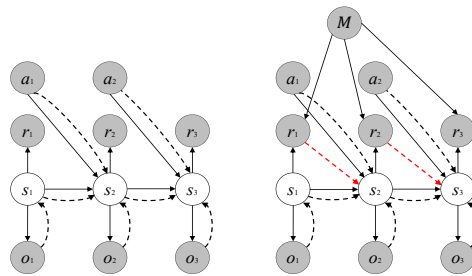
emerge. One primary source of these challenges is the congruence in the underlying dynamics of different tasks, which exhibit distinct reward structures. To illustrate, two tasks might involve navigating a robot, but in one, the robot is rewarded for speed, while in the other, it is rewarded for caution. This tendency towards specialization harms the wider applicability of DRL in real-world scenarios. Developing generalizable agents that recognize and handle these subtle variations continues to be an area of keen interest and exploration in DRL.

For designing such generalizable agents, a promising pathway is to train a general world model [Ha and Schmidhuber, 2018; Hafner *et al.*, 2019b] that helps the agent understand the world and make the decision. In this research, we first provide insight into how a unified dynamic model can help improve the sample efficiency in handling the distribution of tasks, especially by utilizing similar structures of trajectories sampled from different tasks (Theorem 1). Consequently, we propose a novel framework named Task Aware Dreamer (TAD), which extends existing world models into the task generalization setting. As current world models are primarily designed for the single-task setting (left of Fig. 1(b)), we consider the corresponding probabilistic graphical model of the task distribution setting (right of Fig. 1(b)) and extend single-task world model into novel reward-informed world models, which can capture learnable structures in the task distribution. To optimize these models, we compute the variational lower bound of the data log-likelihood while incorporating a novel term that categorizes tasks based on their states, serving as the primary training objective for the reward-informed world models.

Furthermore, we conduct detailed analyses of the components of TAD, which are simple but effective for handling task distribution. First, we point out that the reward-informed policy used in TAD is necessary for task generalization. While prior studies [Ghosh *et al.*, 2021] have highlighted that generalizing to unseen environments results in partial observability, rendering all Markovian policies suboptimal, they often overlook the relationship between the task distribution and the expressiveness of the chosen policy hypothesis set. To bridge this gap, we propose a novel metric of Task Distribution Relevance (TDR), which encapsulates the relevance of different tasks within the distribution through their optimal Q functions. Furthermore, we prove that both the commonly adopted hypothesis set Π_1 of Markovian policies and the set Π_2 of policies that encode historical states and actions, are



(a) Overview of this work



(b) Probabilistic graphical model designs

Figure 1: (a) **An overview.** Given a task distribution, we train the agent in training tasks and hope it to zero-shot generalize to testing tasks. For improving the generalization, we propose TAD, which utilizes Π_3 to encode all historical information for inferring the current task and novel reward-informed world models for capturing invariant latent features. (b) Probabilistic graphical model designs for the single-task setting (**left**) and the task-distribution setting (**right**). The latter inspires the design of reward-informed world models. Solid and dashed lines represent the *generative process* and the *inference model*, respectively.

sub-optimal under the task-distribution setting and struggle to generalize. This sub-optimality is proven to be related to TDR (Theorem 3), i.e., for task distributions with high TDR, the performance of these two policy hypotheses might degenerate significantly as they fail to identify the current task, a phenomenon we also demonstrate by experiments (Sec. 5.2). Consequently, the reward-informed policy hypothesis Π_3 utilized in TAD is necessary for handling task generalization. Besides the policy chosen, we also discuss the novel optimization term, i.e., categorizing tasks based on hidden state, in TAD and theoretically show that it can effectively reduce the gap between the policy return and the optimal return (Theorem 4).

Extensive experiments are performed on task distributions based on DeepMind control suite [Tassa *et al.*, 2018] and MuJoCo simulator [Todorov *et al.*, 2012], which are image-based and state-based respectively. Agents are trained on specific tasks and evaluated for their generalization capabilities on unseen evaluation tasks. Our findings corroborate our analyses, indicating that Π_1 and Π_2 falter in managing task distributions characterized by a high TDR. Contrastingly, TAD excels in discerning and simultaneously managing varied tasks, significantly surpassing benchmark performance. This underscores TAD’s impressive sample efficiency and adaptability in both image-based and state-based contexts. Additionally, our ablation studies spotlight TAD’s versatility, showcasing its prowess in dynamic generalization and handling cross-embodiment tasks. In summary, our contributions are:

- We present a theoretical observation that a general world model can utilize similar structures of different tasks and improve the sample efficiency for training a generalizable agent for the task distribution.
- Extending existing single-task world models into the task distribution setting, we then formulate a new algorithm, termed TAD, leveraging the variational lower bound for calculations and showcasing superior generalization capabilities in contrast to baselines.
- To analyze TAD’s components, we analyze policy generalization across task distributions and introduce a new metric TDR, which quantifies the distribution relevance. Our findings indicate that Markovian policies tend to be sub-optimal, with performance gaps correlating with

TDR. Further, we demonstrate that the new optimization term in TAD is effective for task generalization.

2 Related Work

2.1 Generalization in Reinforcement Learning

Contemporary RL methodologies consistently struggle when tasked with generalizing to new environments [Song *et al.*, 2019]. Prior studies have crafted an array of training methodologies, such as loss regularization [Cobbe *et al.*, 2019; Wang *et al.*, 2020], successor representation [Touati and Olivier, 2021; Touati *et al.*, 2022], network architecture design [Lee *et al.*, 2019; Raileanu and Fergus, 2021], and data augmentation [Raileanu *et al.*, 2021; Hansen and Wang, 2021]. Despite this, there are few investigations into the mechanism behind policy generalization in unseen environments and its relationship with the distribution of those environments. Ghosh *et al.* took the initial step in demonstrating that generalizing to unseen environments introduces partial observability, thereby rendering deterministic Markovian policies *sub-optimal*. Also, some studies [Lee *et al.*, 2020; Ghosh *et al.*, 2021] have experimentally indicated that stochastic or non-Markovian policies can yield superior generalization compared to deterministic Markovian policies. Nevertheless, expressive capabilities of differing hypothesis sets and their connection to the environment distribution remain understudied areas. This knowledge gap is significant for understanding current algorithms and the design of more robust algorithms with enhanced generalization capacities.

There are several topics closely related to generalization, like multi-task RL and meta RL. Multi-task RL [Yang *et al.*, 2020; Sodhani *et al.*, 2021; Lee *et al.*, 2022] primarily aims for the trained agent to excel across all training tasks. For boosting the generalization, Meta RL seeks to enable the trained agents to adapt to new tasks with as little data as possible, including gradient-based [Finn *et al.*, 2017] and context-based methods [Duan *et al.*, 2016; Rakelly *et al.*, 2019]. There are also some model-based methods [Nagabandi *et al.*, 2018; Clavera *et al.*, 2018; Zhao *et al.*, 2021] utilize learned models to boost the sample efficiency. Though some context-based methods like VariBAD [Zintgraf *et al.*, 2019] show zero-shot generalization ability, it is still significant to analyze the generalization in RL and design corresponding algorithms.

2.2 World Models

The concept of world models [Ha and Schmidhuber, 2018] aims to better learn environmental representations, which has potential advantages for generalization as it can capture invariant features across tasks. Classical methods utilize the Recurrent State Space Model (RSSM) [Hafner *et al.*, 2019b] for planning like PlaNet [Hafner *et al.*, 2019b] and policy learning like Dreamer [Hafner *et al.*, 2019a; Hafner *et al.*, 2020; Hafner *et al.*, 2023]. Subsequent research explored reconstruction-free world models [Deng *et al.*, 2022], preserving representational capacity by avoiding reconstructing task-irrelevant elements. Also, techniques like temporal predictive coding [Nguyen *et al.*, 2021], cooperative reconstruction [Fu *et al.*, 2021], and Denoised MDP [Wang *et al.*, 2022] have been proposed for more effective task-relevant information encoding. Recent works [Chen *et al.*, 2021; Robine *et al.*, 2023] integrate Transformer [Vaswani *et al.*, 2017] into world models for capturing long-term dependencies. Other studies propose using world models to extract environmental invariant features by learning from videos [Seo *et al.*, 2022] or exploration [Sekar *et al.*, 2020; Xu *et al.*, 2022], and then fine-tuning to new tasks. However, most world models are designed for the single-task setting and struggle to manage multiple tasks without fine-tuning, limiting their effectiveness for zero-shot generalization to unseen tasks.

3 Preliminary

We consider the setting with a task distribution \mathcal{T} of MDPs, where different tasks own the same dynamic and different rewards. Formally, each MDP $\mathcal{M} \sim \mathcal{T}$ is represented as $\mathcal{M} = (\mathcal{S}, \mathcal{A}, \mathcal{P}, \mathcal{R}_{\mathcal{M}}, \gamma)$. Here \mathcal{S} and \mathcal{A} denote the state and action spaces, respectively. For $\forall (s, a) \in \mathcal{S} \times \mathcal{A}$, $\mathcal{P}(\cdot|s, a)$ is a distribution over \mathcal{S} , representing the dynamic, $\mathcal{R}_{\mathcal{M}}(s, a)$ is the reward function of \mathcal{M} , and $\gamma \in (0, 1)$ is a discount factor.

Although deterministic Markovian policy is well known to be optimal for handling the single task setting, some recent work [Ghosh *et al.*, 2021] has demonstrated that generalizing to unseen environments introduces partial observability, thus deterministic Markovian policy will be sub-optimal and we need to encode more historical information. Also, previous multi-task methods [Rakelly *et al.*, 2019; Zintgraf *et al.*, 2019] will utilize all historical information to choose the action. Formally, given policy π , at each timestep t , the agent will use the whole history trajectory $(s_0, a_0, r_0, s_1, a_1, \dots, s_t)$ to sample action a_t , arrive at the next state $s_{t+1} \sim \mathcal{P}(\cdot|s_t, a_t)$, and get the current reward $r_t = \mathcal{R}_{\mathcal{M}}(s_t, a_t)$. The performance of policy π in \mathcal{M} is defined as the expected discounted return of the trajectory τ : $J_{\mathcal{M}}(\pi) = \mathbb{E}_{\tau \sim \pi} [R(\tau) \triangleq \sum_{t=0}^{\infty} \gamma^t r_t]$, where $R(\tau)$ represents the discounted return of τ . And we hope to find the optimal policy over \mathcal{T} , i.e., $\max_{\pi} \mathbb{E}_{\mathcal{M} \sim \mathcal{T}} [J_{\mathcal{M}}(\pi)]$.

In practice, given the task distribution \mathcal{T} , we sample M training tasks $\{\mathcal{M}_m\}_{m=1}^M$ for optimizing the agent, i.e., maximizing $\frac{1}{M} \sum_{m=1}^M J_{\mathcal{M}_m}(\pi)$. In the testing stage, we will sample N unseen testing tasks $\{\mathcal{M}_{M+n}\}_{n=1}^N$ to evaluate its generalization ability, i.e., evaluating $\frac{1}{N} \sum_{n=1}^N J_{\mathcal{M}_{M+n}}(\pi)$.

4 Task Aware Dreamer

In this section, we propose a novel framework of Task Aware Dreamer (TAD) for handling task generalization, including the reward-informed world models and the optimization. Finally, we will provide theoretical analyses of designs in TAD.

4.1 Reward-Informed World Models

Our first observation is that model-based methods, in addition to proving to improve sample efficiency in the single-task setting [Janner *et al.*, 2019; Hafner *et al.*, 2019a], are also effective in narrowing down the hypothesis space of the optimal Q function when considering task generalization:

Theorem 1 (Informally, a detailed version and proof are in Appendix B.1). *Given M tasks $\{\mathcal{M}_m\}_{m=1}^M$ and corresponding dataset D^m sampled from \mathcal{M}_m . We can consider three hypothesis classes of optimal Q function $\mathcal{H}_1, \mathcal{H}_2, \mathcal{H}_3$ as*

- \mathcal{H}_1 includes all optimal Q functions satisfying the Bellman optimality equation for all transitions in \mathcal{D}_m .
- For any dynamics p_m satisfying the dynamic transition in \mathcal{D}_m , \mathcal{H}_2 includes all optimal Q functions satisfying the Bellman optimality equation for all transitions consistent with p_m .
- For any dynamics p satisfying all dynamic transition in $\{\mathcal{D}_m\}_{m=1}^M$, \mathcal{H}_3 includes all optimal Q functions satisfying the Bellman optimality equation for all transitions consistent with p .

We have that $\mathcal{H}_3 \subseteq \mathcal{H}_2 \subseteq \mathcal{H}_1$.

Here $\mathcal{H}_2 \subseteq \mathcal{H}_1$ utilizes the generalization ability of the trained world model, which is similar to the single-task setting. Moreover, $\mathcal{H}_3 \subseteq \mathcal{H}_2$ is based on similar dynamic structures across different tasks, which benefits learning the general world model. In summary, this result inherits the previous result [Young *et al.*, 2022] where the reward function is unchanged and inspires us that training a general world model can narrow down the hypothesis of possible Q function as well as benefit training the agent.

As traditional world models [Hafner *et al.*, 2019b; Hafner *et al.*, 2019a] mainly designed for the single-task setting, we first analyze the probabilistic graphical model of the task-distribution setting in Fig. 1(b) and further build reward-informed world models for handling the task distribution. As shown in Fig. 1(b), the reward does not only rely on the previous states and actions but also on the current task. Thus the joint distribution can be calculated as

$$p(s_{1:T}, o_{1:T}, r_{1:T}, a_{1:T-1}, \mathcal{M}) = p(\mathcal{M}) \prod_{t=1}^T p(s_{t+1}|s_t, a_t) p(o_t|s_t) p(r_t|s_t, \mathcal{M}), \quad (1)$$

and we choose the reward-informed inference model (analyses about the necessity of utilizing reward-informed policy in task generalization is in Sec. 4.3) to approximate state posteriors as

$$q(s_{1:T}|o_{1:T}, a_{1:T}, r_{1:T}) = \prod_{t=1}^T q(s_t|s_{t-1}, a_{t-1}, r_{t-1}, o_t). \quad (2)$$

Further, we can construct the variational lower bound of the log-likelihood on the data as

$$\begin{aligned} & \ln p(o_{1:T}, r_{1:T}, \mathcal{M}|a_{1:T}) \\ \geq & \sum_{t=1}^T \mathbb{E}_{q(s_t|o_{\leq t}, a_{\leq t}, r_{\leq t})} [\ln p(o_t, r_t | \mathcal{M}, s_t)] \\ & - \text{KL}(q(s_t|o_{\leq t}, r_{\leq t}, a_{\leq t}) \| p(s_t|s_{t-1}, a_{t-1})) \\ & + \mathbb{E}_{q(s_{1:T}|o_{1:T}, a_{1:T}, r_{1:T})} [\ln p(\mathcal{M}|s_{1:T})]. \end{aligned} \quad (3)$$

It is a general form of the single task setting [Hafner *et al.*, 2019b] and the detailed derivation is in Appendix B.2. Here the first two terms in Eq.(3) are for reconstructing observations, predicting rewards, and inferring states, which are similar to the single-task setting. The last novel term is dedicated to predicting the current task from historical information, which is beneficial for improving the generalization as it encourages inferring the current task context, and we use one-hot task vectors to present \mathcal{M} during training. Extending RSSM via Eq.(3), our reward-informed world models consist of:

$$\begin{aligned} \text{Deterministic state model:} & \quad h_t = f(h_{t-1}, s_{t-1}, a_{t-1}, r_{t-1}), \\ \text{Transition model:} & \quad p_\theta(s_t|h_t), \\ \text{Observation model:} & \quad p_\theta(o_t|h_t, s_t), \\ \text{Reward model:} & \quad p_\theta(r_t|h_t, s_t), \\ \text{Task model:} & \quad p_\theta(\mathcal{M}|h_t, s_t). \end{aligned}$$

Here hidden state h_t encodes historical states, actions, and rewards, by using gated recurrent unit (GRU) [Chung *et al.*, 2014] as $f(\cdot) = \text{GRU}(\cdot)$. Then the transition model, observation model, and reward model further predict state, observation, and reward respectively. Finally, the task model infers the current task to distinguish different tasks' trajectories.

4.2 Optimization

Based on the above analyses, we now introduce the training of TAD in detail. Following previous work [Hafner *et al.*, 2019a], we adopt an alternating training approach between the reward-informed world models and the policy.

To balance different tasks, in the stage of collecting data, TAD utilizes different replay buffers $\{\mathcal{D}_m\}_{m=1}^M$ to store trajectories sampled from $\{\mathcal{M}_m\}_{m=1}^M$, respectively. Then in the training stage, TAD will sample data from each replay buffer and train the reward-informed world models via the objective, which follows Eq. (3), as

$$\begin{aligned} L_{\text{TAD}} = & \sum_{i=1}^M \mathbb{E}_q \left[\sum_{t=1}^T \ln p_\theta(o_t^i|h_t^i, s_t^i) + \sum_{t=1}^T \ln p_\theta(r_t^i|h_t^i, s_t^i) \right. \\ & \left. - \sum_{t=1}^T D_{\text{KL}}(q(s_t^i|h_t^i, o_t^i) \| p_\theta(s_t^i|h_t^i)) + \sum_{t=1}^T \ln p_\theta(\mathcal{M}_i|h_t^i, s_t^i) \right]. \end{aligned} \quad (4)$$

In Eq. (4), the first three items are similar to Dreamer for reconstructing observations, predicting rewards, and inferring states. The novel last term is calculated in Eq. (3) for encouraging the agent to encode task information into hidden states and infer the current task based on these hidden states, which

Algorithm 1 Task Aware Dreamer (TAD)

Require: M training tasks $\{\mathcal{M}_m\}_{m=1}^M$, M replay buffers $\{\mathcal{D}_m\}_{m=1}^M$, N testing tasks $\{\mathcal{M}_{M+n}\}_{n=1}^N$, initialize parameters of world models, the policy, and the critic.

- 1: **while** not converge **do**
 - 2: **for** update step = 1, 2, ..., U **do**
 - 3: Sample o - a - r pairs $\{(o_t^i, a_t^i, r_t^i)_{t=1}^T\}$ from each replay buffer $\mathcal{D}_i, i = 1, 2, \dots, M$
 - 4: Calculate the deterministic state h and further calculate model states s .
 - 5: Update the world models via optimizing Eq. (4).
 - 6: Collect imagined trajectories from each s via the policy and the world models and use these imagined trajectories to update the policy and the critic.
 - 7: **end for**
 - 8: Collect trajectories from $\mathcal{M}_m (m = 1, 2, \dots, M)$ and store them into the replay buffer \mathcal{D}_m .
 - 9: **end while**
 - 10: Evaluate the agent in testing environments $\{\mathcal{M}_{M+n}\}$.
-

benefits generalizing to unseen tasks (We demonstrate this in Sec. 4.3).

In terms of training the actor-critic, both of which are parameterized neural networks, we follow the actor-critic learning approach in Dreamer with a more powerful hypothesis set Π_3 (The necessity is shown in Sec. 4.3). When optimizing the policy, TAD samples a series of states from the replay buffer and starts from them to imagine trajectories via interacting with reward-informed world models, which is fixed at this time. Here reward-informed world models can capture invariant features, which are beneficial for the agent to train more effectively and gain better generalization. After obtaining imagined trajectories, the actor-critic can be optimized via maximizing the λ -return [Schulman *et al.*, 2015] and regressing the targets calculated by TD [Sutton and Barto, 2018], respectively.

4.3 Theoretical Analyses

In this part, we will provide some analyses to show that components of TAD are simple but effective for task generalization.

Is it necessary to use policies that utilize all historical information for task generalization? Below we will introduce 3 types of widely used policy hypotheses and show that Π_3 , used in TAD, is necessary for handling the task generalization.

1. Markovian policy set Π_1 [Sutton and Barto, 2018; Yarats *et al.*, 2021], i.e., $\Pi_1 = \{\pi | \pi : \mathcal{S} \rightarrow \Delta(\mathcal{A})\}$, here $\Delta(\mathcal{A})$ represents a distribution over \mathcal{A} , which is widely used and optimal for the single-task setting;
2. \mathcal{S} - \mathcal{A} memorized policy set Π_2 [Hafner *et al.*, 2019a; Hafner *et al.*, 2020; Lee *et al.*, 2020], i.e., $\Pi_2 = \{\pi | \pi : \mathcal{H} \rightarrow \Delta(\mathcal{A})\}$, here $\mathcal{H} = \cup_{t=1}^\infty \mathcal{H}_t, \mathcal{H}_t = (\mathcal{S} \times \mathcal{A})^{t-1} \times \mathcal{S}$;
3. \mathcal{S} - \mathcal{A} - \mathcal{R} memorized policy set Π_3 [Rakelly *et al.*, 2019; Zintgraf *et al.*, 2019], i.e., $\Pi_3 = \{\pi | \pi : \mathcal{L} \rightarrow \Delta(\mathcal{A})\}$, here $\mathcal{L} = \cup_{t=1}^\infty \mathcal{L}_t, \mathcal{L}_t = (\mathcal{S} \times \mathcal{A} \times \mathbb{R})^{t-1} \times \mathcal{S}$.

As illustrated in Fig. 1(a), naturally $\Pi_1 \subseteq \Pi_2 \subseteq \Pi_3$. Next, we will analyze their expressive ability under task distribution \mathcal{T} . Denote $J_{\mathcal{T}}^* \triangleq \mathbb{E}_{\mathcal{M} \sim \mathcal{T}} [\max_{\pi} J_{\mathcal{M}}(\pi)]$ as the optimal return

under \mathcal{T} , and $J_{\mathcal{T}}^i \triangleq \max_{\pi \in \Pi_i} [\mathbb{E}_{\mathcal{M} \sim \mathcal{T}} J_{\mathcal{M}}(\pi)]$ as the optimal return for $\Pi_i (i = 1, 2, 3)$ under \mathcal{T} . Our first main result shows that, although $\Pi_1 \subseteq \Pi_2$, they own the same expressive ability, i.e., $J_{\mathcal{T}}^1 = J_{\mathcal{T}}^2$, and are both *sub-optimal*, summarized as:

Theorem 2 (Sub-Optimality of Π_1, Π_2 . Proof in Appendix B.3). *We set $\mathcal{M} = (\mathcal{S}, \mathcal{A}, \mathcal{P}, \mathcal{R}, \gamma)$, here $\mathcal{R} = \mathbb{E}_{\mathcal{M} \sim \mathcal{T}}[\mathcal{R}_{\mathcal{M}}]$. For $\forall \pi \in \Pi_2$, we have $\mathbb{E}_{\mathcal{M} \sim \mathcal{T}}[J_{\mathcal{M}}(\pi)] = J_{\bar{\mathcal{M}}}(\pi)$ and further $J_{\mathcal{T}}^1 = J_{\mathcal{T}}^2 \leq J_{\mathcal{T}}^*$.*

Theorem 2 reveals that the cumulative returns of policies in Π_1 and Π_2 are the same as their returns in the ‘‘average’’ MDP \mathcal{M} , where the reward function is the average of reward functions in different tasks. Also, as Π_1 and Π_2 only choose actions via current state or historical state-action pairs, they cannot distinguish different tasks and are both *sub-optimal*.

To quantitatively analyze the characteristic of \mathcal{T} and the gap between $J_{\mathcal{T}}^1, J_{\mathcal{T}}^2$ and $J_{\mathcal{T}}^*$, we propose a novel metric named Task Distribution Relevance (TDR) of the distribution \mathcal{T} as

Definition 1 (Task Distribution Relevance). *For any task distribution \mathcal{T} and state s , the Task Distribution Relevance of \mathcal{T} and s is defined as*

$$D_{TDR}(\mathcal{T}, s) = \mathbb{E}_{\mathcal{M} \sim \mathcal{T}}[\max_a Q_{\mathcal{M}}^*(s, a)] - \max_a \mathbb{E}_{\mathcal{M} \sim \mathcal{T}}[Q_{\mathcal{M}}^*(s, a)]. \quad (5)$$

Intuitively, TDR describes the relevance of \mathcal{T} via optimal Q functions, which determine the distribution of optimal actions in corresponding tasks. Based on TDR, we can bound the gap:

Theorem 3 (Proof in Appendix B.4). *Assume $\pi_{\mathcal{M}}^* = \arg \max_{\pi} J_{\mathcal{M}}(\pi)$, for $\forall \pi \in \Pi_1$, we have*

$$J_{\mathcal{T}}^* - \mathbb{E}_{\mathcal{M} \sim \mathcal{T}}[J_{\mathcal{M}}(\pi)] \geq \frac{1}{1 - \gamma} \mathbb{E}_{s \sim d_{\mathcal{M}, \pi}}[D_{TDR}(\mathcal{T}, s)] \quad (6)$$

Thus $J_{\mathcal{T}}^* - J_{\mathcal{T}}^2 = J_{\mathcal{T}}^* - J_{\mathcal{T}}^1 \geq \frac{1}{1 - \gamma} \mathbb{E}_{s \sim d_{\mathcal{M}, \pi^*}}[D_{TDR}(\mathcal{T}, s)]$, here $\pi^* = \arg \max_{\pi \in \Pi_1} J_{\mathcal{M}}(\pi)$.

Theorem 3 demonstrates that the gap between $J_{\mathcal{T}}^1, J_{\mathcal{T}}^2$ and $J_{\mathcal{T}}^*$ is related to the TDR of \mathcal{T} . When considering \mathcal{T} with high TDR, i.e., the optimal Q values in different tasks differ greatly, the performance of Π_1 and Π_2 will be extremely poor since they cannot differentiate different tasks and their expressive abilities are significantly limited. This conclusion is further verified empirically in the experimental section. Moreover, we can show that $J_{\mathcal{T}}^1, J_{\mathcal{T}}^2$ might be arbitrarily small when $J_{\mathcal{T}}^3$ might be arbitrarily close to $J_{\mathcal{T}}^*$ (More details are in Appendix B.5), which demonstrates that Π_3 owns stronger expressive ability. Consequently, it is necessary to utilize Π_3 to distinguish different tasks for enhancing expression ability and generalization over the task distribution.

Is optimizing $p_{\theta}(\mathcal{M}|h_t, s_t)$ helpful for task generalization? Now we will show that, although $p_{\theta}(\mathcal{M}|h_t, s_t)$ is a simple term, optimizing it can be effective for reaching the generalizable agent in the task distribution.

As the input space of Π_3 is \mathcal{L} , i.e., all partial trajectories, our major result analyzes the relation between the policy $\pi \in \Pi_3$ and the task posterior $p(\mathcal{M}|l), l \in \mathcal{L}$. Notice that $p_{\theta}(\mathcal{M}|h_t, s_t)$ can be regard a deformation of $p(\mathcal{M}|l), l \in \mathcal{L}$ as h_t encodes all historical information.

Theorem 4 (Informally, detailed analyses and proof are in Appendix B.6). *For any policy $\pi \in \Pi_3$, we have*

$$J_{\mathcal{T}}^* - \mathbb{E}_{\mathcal{M} \sim \mathcal{T}}[J_{\mathcal{M}}(\pi)] = \frac{1}{1 - \gamma} \int_{\mathcal{L}} p(l) dl \left[\int p(\mathcal{M}|l) \max_a Q_{\mathcal{M}}^*(l, a) d\mathcal{M} - \max_a \int p(\mathcal{M}|l) Q_{\mathcal{M}}^*(l, a) d\mathcal{M} \right], \quad (7)$$

here $p(l)$ is a distribution of \mathcal{L} related to \mathcal{T}, π and $p(\mathcal{M}|l)$ is the task posterior related to π .

Consequently, maximizing $p(\mathcal{M}|l)$, i.e., making the distribution of $p(\mathcal{M}|l)$ to be closer to some Dirac distribution, can significantly reduce the right part of Eq. (7), thus is effective for improving the generalization ability of π . More details and discussion are also provided in Appendix B.6.

5 Experiments

We now present empirical results to answer the questions:

- Can we verify the analyses about TDR, i.e., the expressive abilities of Π_1, Π_2 are severely restricted in task distributions with high TDR?
- What about the generalization ability of TAD in both image-based and state-based environments?
- Can TAD be extended to more general settings like dynamic generalization?

5.1 Experimental Setup

Image-based Control. To answer the first question and verify analyses about TDR, we first consider lots of different task combinations in DeepMind control suite (DMC) [Tassa *et al.*, 2018]. These task combinations include (1) two task combinations of **Walker-stand&walk** [Mu *et al.*, 2022] and **Acrobot-swingup&sparse**, which share the same optimal actions with TDR being 0; (2) two task combinations with non-zero TDR of **Reacher-easy&hard** [Mu *et al.*, 2022] and **Walker-walk&prostrate**. For example, Walker-walk and Walker-prostrate hope a two-leg robot to maintain its height above a certain threshold for walking and below another certain threshold respectively, yielding almost opposite optimal Q functions with huge TDR. In **Appendix C.1**, we introduce more details about them and four other task combinations.

To evaluate generalization, we extend tasks in DMC and design three task distributions: (1) **Cheetah-speed**(α, β), which extends Cheetah-run and hopes the agent to run within the target speed interval ($\alpha - \beta, \alpha + \beta$); (2) **Pendulum-angle**(α, β), which extends Pendulum-swingup and hopes an inverted pendulum to stay its pole within the target angle interval ($\arccos \alpha, \arccos \beta$); and (3) **Walker-speed**(α, β), which is based on Walker-run and requires the planar walker to run within the target speed interval ($\alpha - \beta, \alpha + \beta$). For each task distribution, we sample 4 tasks for training and 2 additional tasks for testing. More details are in **Appendix C.2**.

State-based Control. To demonstrate the scalability of TAD, we also consider some state-based continuous control task distributions about robotic locomotion, simulated via the MuJoCo simulator [Todorov *et al.*, 2012]. Following previous

Tasks	Hypothesis	Walker-stand&walk	Acrobot-swingup&sparse	Reacher-easy&hard	Walker-walk&prostrate
CURL	Π_1	563.4 \pm 16.0	11.0 \pm 1.8	552.5 \pm 88.9	441.0 \pm 7.7
SAC+AE	Π_1	683.8 \pm 164.3	11.7 \pm 5.4	669.5 \pm 99.4	445.8 \pm 2.6
PlaNet	Π_2	990.6 \pm 3.8	12.2 \pm 9.8	341.0 \pm 228.3	445.4 \pm 5.1
Dreamer	Π_2	992.3 \pm 1.7	159.9 \pm 108.4	506.1 \pm 382.9	449.7 \pm 12.5
TAD	Π_3	993.9 \pm 1.0	217.3 \pm 107.1	823.3 \pm 237.4	913.7 \pm 11.5

Table 1: Performance (mean \pm std) over different task combinations in image-based DMC of the best policy. Numbers greater than **95** % of the best performance for each environment are **bold**.

Tasks	Hypothesis	Cheetah_speed		Pendulum_angle		Walker_speed	
		Train	Test	Train	Test	Train	Test
CURL	Π_1	211.7 \pm 13.7	57.4 \pm 26.6	137.1 \pm 8.6	57.4 \pm 21.8	127.0 \pm 33.7	77.5 \pm 11.5
SAC+AE	Π_1	182.2 \pm 7.6	115.2 \pm 10.1	144.0 \pm 4.5	68.6 \pm 3.7	136.8 \pm 34.4	27.5 \pm 10.5
PlaNet	Π_2	176.6 \pm 25.9	83.0 \pm 52.2	99.8 \pm 28.3	80.5 \pm 24.2	173.9 \pm 19.3	58.4 \pm 23.7
Dreamer	Π_2	250.2 \pm 9.6	3.0 \pm 2.2	92.2 \pm 19.9	79.6 \pm 14.8	197.6 \pm 24.6	10.0 \pm 6.5
TAD	Π_3	951.9 \pm 3.3	876.9 \pm 51.1	344.8 \pm 2.8	132.6 \pm 14.2	241.2 \pm 36.8	156.5 \pm 129.6

Table 2: Generalization performance (mean \pm std) over different task distributions in image-based DMC of the best policy. Numbers greater than **95** % of the best performance for each environment are **bold**.

Tasks	Hypothesis	Half-Cheetah-Fwd-Back(1e7)		Half-Cheetah-Vel(1e7)		Humanoid-Direc-2D(1e6)	
		Train&Test	Test	Train	Test	Train	Test
PlaNet	Π_2	30.5 \pm 42.9	—	-198.1 \pm 1.9	-202.1 \pm 1.8	215.9 \pm 72.3	220.6 \pm 75.3
Dreamer	Π_2	127.4 \pm 181.8	—	-151.4 \pm 0.4	-169.4 \pm 1.2	260.5 \pm 48.9	191.9 \pm 52.3
RL2(zero-shot)	Π_3	1070.7 \pm 109.7	—	—	-70.3 \pm 6.7	—	191.9 \pm 50.8
RL2(few-shot)	Π_3	1006.9 \pm 26.4	—	—	-146.9 \pm 0.4	—	268.8 \pm 30.2
MAML(few-shot)	—	429.3 \pm 81.4	—	—	-121.0 \pm 37.1	—	205.3 \pm 34.7
VariBAD(zero-shot)	Π_3	1177.5 \pm 94.9	—	—	-58.4 \pm 20.6	—	260.3 \pm 61.6
TAD	Π_3	1455.8 \pm 78.3	—	-49.3 \pm 1.9	-47.1 \pm 0.3	339.5 \pm 78.7	335.5 \pm 70.5

Table 3: Generalization performance (mean \pm std) over different task distributions in state-based MuJoCo of the best policy. Numbers greater than **95** % of the best performance are **bold**.

work [Finn *et al.*, 2017], our chosen tasks distributions include (1) **Half-Cheetah-Fwd-Back**, which owns two opposite tasks; and (2) **Half-Cheetah-Vel** and **Humanoid-Direc-2D**, which are task distributions with 100 training tasks 30 testing tasks. More details of these task distributions are in **Appendix D**.

Baselines. In DMC, we choose two model-free methods: CURL [Laskin *et al.*, 2020] and SAC+AE [Yarats *et al.*, 2021], which employ Markovian policies and belong to Π_1 . In addition, we choose two classic world models, PlaNet [Hafner *et al.*, 2019b] and Dreamer [Hafner *et al.*, 2019a], which utilize historical state-actions in policies and belong to Π_2 . In state-based control, besides PlaNet and Dreamer, we also take some meta RL methods like MAML [Finn *et al.*, 2017], RL2 [Duan *et al.*, 2016], and VariBAD [Zintgraf *et al.*, 2019], including zero-shot and few-shot evaluation, as reference.

Metrics. For the task combinations, we evaluate the average return of all tasks to verify TDR. For the task generalization setting, we train agents in training tasks and evaluate their generalization abilities in testing tasks. For all experiments, we train 3 policies with different seeds and calculate the mean and std to mitigate the effects of randomness.

5.2 Experimental Results for TDR

To answer the first question and validate our analyses of TDR, we report the optimal mean \pm std of the average cumulative return of different task combinations in Table 5. Comprehensive results of all 8 task combinations and training curves are in **Appendix C.3**. The results show that TAD outperforms

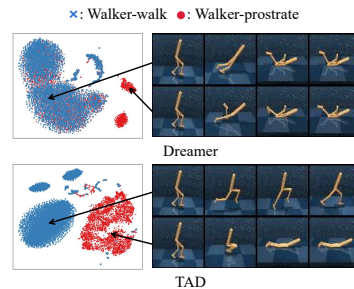


Figure 2: Visualization of Dreamer (upper) and TAD (lower) for handling Walker-walk&Prostrate. For each algorithm in each task, we show 4 frame observations of a trajectory in the right part. In the left part, we draw t-SNE results of all states in trajectories of Walker-walk (blue points) and Walker-prostrate (red points).

baselines in all environments, especially in those with high TDR. In task combinations where TDR is 0, like Walker-stand&walk or Acrobot-swingup&sparse, different tasks share the same optimal action and Π_1 , Π_2 own the optimal policy, as derived in Theorem 3. In these cases, Π_1 , Π_2 performs well and TAD can surpass baselines in Acrobot-swingup&sparse since it can better distinguish different tasks. In the latter two environments with non-zero TDR, TAD achieves a notable improvement compared with baselines. Especially, in Walker-walk&prostrate, where two tasks own almost opposite optimal Q functions and TDR is significantly huge, policies belong to Π_1 , Π_2 and can not differentiate different tasks, aligning with our Theorem 3. In contrast, TAD can distinguish between tasks by utilizing Π_3 and improves performance conspicuously.

Tasks	Acrobot-Cartpole-Pendulum	Walker-Cheetah-Hopper	Cheetah-run_mass		Walker-walk_mass	
	Train&Test	Train&Test	Train	Test	Train	Test
Dreamer	541.3 \pm 4.0	299.4 \pm 17.2	717.8 \pm 27.9	711.7 \pm 38.8	889.9 \pm 114.1	903.3 \pm 102.8
TAD	667.7 \pm 6.4	554.7 \pm 23.6	754.3 \pm 22.9	738.2 \pm 41.1	957.8 \pm 35.1	963.1 \pm 32.6

Table 4: Generalization performance (mean \pm std) over different task distributions in image-based DMC of the best policy. Numbers greater than **95** % of the best performance for each environment are **bold**.

Moreover, we present some visualization to better understand how TAD works in Fig. 2. We sample trajectories from the trained agent via Dreamer as well as TAD in Walker-walk&prostrate and visualize some observations (right part of Fig. 2) as well as all states (left part of Fig. 2), of which the dimensions are reduced for visualization by t-SNE [Van der Maaten and Hinton, 2008]. As shown here, states in TAD of different tasks are clearly distinguished, while Dreamer can not differentiate them and perform the same in different tasks. Consequently, TAD can successfully distinguish different tasks and handle them at the same time effectively. Videos of these trajectories are in supplementary materials.

5.3 Experimental Results for Task Generalization

To answer the second question, we report the results under the task generalization setting of image-based and state-based environments in Table 2 and Table 3, respectively. In Table 2, TAD shows powerful generalization ability in image-based environments as it can significantly enhance the average cumulative return in both training tasks and testing tasks compared with baselines. This demonstrates that TAD can both handle multiple training tasks simultaneously and generalize to unseen testing tasks effectively. We also provide some visualization results in Appendix C.4 with corresponding videos in supplementary materials.

Additionally, in Table 3, we compare TAD with some meta RL methods in state-based environments, of which the training timesteps are $1e7$, $1e7$, and $1e6$, respectively. Many context-based meta-RL methods, including RL2, PEARL and VariBAD, utilize reward into policies and belong to Π_3 , thus they can distinguish different tasks, which also verify our analyses. As shown in Table 3, TAD can achieve a significant improvement in the average cumulative return for both training tasks and testing tasks, since TAD is aware of task information and can generalize to unseen tasks.

5.4 Ablation Study

Reward Signal and Task ID. In Fig. 3, we do ablation studies with two baselines: Dreamer(w/ r), which only integrates Π_3 into Dreamer, i.e., including reward signals into policies, and Dreamer(w/ task ID), which includes one-hot task ID into policies in both training and testing. Results show that just providing reward signals can help Dreamer distinguish different tasks, which verifies our analyses in TDR. Also, TAD shows superior performance even compared with Dreamer(w/ task ID), which demonstrates that our task model and corresponding ELBO are effective for task generalization.

Extension to Dynamic Generalization. To answer the third question, we further evaluate TAD in more general settings with different observations, dynamics, and/or actions. As TAD utilizes all historical information to infer the environment, it can be directly applied to these settings. We de-

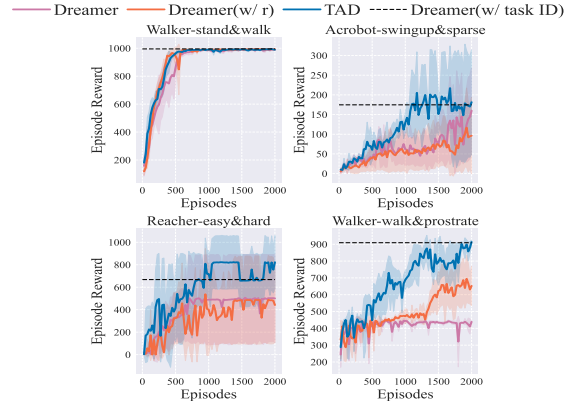


Figure 3: Ablation study on Reward Signal and Task ID.

sign task distribution with different embodiments (Acrobot-Cartpole-Pendulum, Walker-Cheetah-Hopper), as well as different dynamics (Cheetah-run_mass, Walker-walk_mass). Table 4 shows that TAD can achieve much greater performance and better convergence compared to Dreamer, which indicates TAD’s potential in further handling dynamic generalization and even cross-embodiment tasks. More details about the environments and results are in Appendix E.1.

5.5 Limitations and Ethical Statement

In terms of limitations, TAD assumes that the task context is continuously related to historical information for generalizing to unseen tasks. Thus TAD might be difficult to generalize in sparse-reward settings. We further demonstrate that without extra knowledge or finetuning, zero-shot generalization to unseen tasks with extremely sparse rewards is impossible since there is no way to distinguish different tasks (Appendix B.7). Fortunately, in relatively sparse reward settings, we conduct studies in Appendix E.2 to show that TAD can infer the current task and generalize to unseen tasks well. There are no serious ethical issues as this is basic research.

6 Conclusion

In this work, we propose a novel framework of TAD that distinguishes different tasks via all historical information and utilizes novel reward-informed world models to capture invariant latent features. In TAD, we calculate the corresponding variational lower bound of the data log-likelihood, which includes a novel loss term to distinguish different tasks via states. To explain components in TAD, we introduce a novel metric TDR to capture the relevance of the task distribution and show that Markovian policies perform poorly in tasks with high TDR. Experiments in image-based and state-based settings demonstrate that TAD can remarkably improve the performance of handling different tasks meanwhile, especially for high TDR ones, and successfully generalize to unseen tasks.

A Pseudo Code of TAD

We provide the pseudo code of TAD in Algorithm 2.

B Proof of Theorems

In this section, we will provide detailed proofs of theorems.

B.1 The Proof of Theorem 1

In this part, we give an informed version of Theorem 1 with detailed proof as

Theorem 5. *Given M tasks $\{\mathcal{M}_m\}_{m=1}^M$, we consider the product space $\mathcal{H} = \mathcal{Q}^M$ composed of M state- Q function spaces, $\forall \{q_m\}_{m=1}^M \in \mathcal{H}$, $q_m : \mathcal{S} \times \mathcal{A} \rightarrow \mathbb{R}$ is some Q function. Given M corresponding dataset $D^m = \{(s_t^m, a_t^m, r_t^m, s_{t+1}^m)\}$, we can consider three hypothesis classes of optimal Q function $\mathcal{H}_1, \mathcal{H}_2, \mathcal{H}_3$, which are subsets of \mathcal{H} :*

$$\begin{aligned} \mathcal{H}_1 &= \{(q_m)_{m=1}^M \mid q_m(s_t^m, a_t^m) = r_t^m + \gamma \max_{a'} q_m(s_{t+1}^m, a')\} \\ \mathcal{H}_2 &= \{(q_m)_{m=1}^M \mid \exists \{p_m\}_{m=1}^M : p_m(s_t^m, a_t^m) = s_{t+1}^m, \\ &\quad q_m(s, a) = r^m(s, a) + \gamma \max_{a'} q_m(p_m(s, a), a'), \forall s, a\} \\ \mathcal{H}_3 &= \{(q_m)_{m=1}^M \mid \exists p : p(s_t^m, a_t^m) = s_{t+1}^m, \\ &\quad q_m(s, a) = r^m(s, a) + \gamma \max_{a'} q_m(p(s, a), a'), \forall s, a\}. \end{aligned} \quad (8)$$

Then we have $\mathcal{H}_3 \subseteq \mathcal{H}_2 \subseteq \mathcal{H}_1$.

Proof. First, we will show that $\mathcal{H}_2 \subseteq \mathcal{H}_1$, following the proof in [Young *et al.*, 2022] that considers the setting that the rewards of all environments are the same.

$$\begin{aligned} &\{q_m\} \in \mathcal{H}_2 \\ \Leftrightarrow &\exists \{p_m\} : p_m(s_t^m, a_t^m) = s_{t+1}^m, \forall m, t \\ &q_m(s, a) = r^m(s, a) + \gamma \max_{a'} q_m(p_m(s, a), a'), \forall m, s, a \\ \Rightarrow &\exists \{p_m\} : p_m(s_t^m, a_t^m) = s_{t+1}^m, \forall m, t \\ &q_m(s_t^m, a_t^m) = r_t^m + \gamma \max_{a'} q_m(p_m(s_t^m, a_t^m), a'), \forall m, t \\ \Rightarrow &q_m(s_t^m, a_t^m) = r_t^m + \gamma \max_{a'} q_m(p_m(s_t^m, a_t^m), a'), \forall m, t \\ \Leftrightarrow &\{q_m\} \in \mathcal{H}_1, \end{aligned} \quad (9)$$

thus we have $\mathcal{H}_2 \subseteq \mathcal{H}_1$. Next, we prove that $\mathcal{H}_3 \subseteq \mathcal{H}_2$, which is mainly because we can utilize similar dynamic structures from different tasks to narrow down the hypothesis spaces of the dynamic model.

$$\begin{aligned} &\{q_m\} \in \mathcal{H}_3 \\ \Leftrightarrow &\exists p : p(s_t^m, a_t^m) = s_{t+1}^m, \forall m, t \\ &q_m(s, a) = r^m(s, a) + \gamma \max_{a'} q_m(p(s, a), a'), \forall m, s, a \\ \Rightarrow &\exists p_m : p_m(s_t^m, a_t^m) = s_{t+1}^m, \forall m, t \\ &q_m(s, a) = r^m(s, a) + \gamma \max_{a'} q_m(p_m(s, a), a'), \forall m, s, a \\ \Leftrightarrow &\{q_m\} \in \mathcal{H}_2, \end{aligned} \quad (10)$$

thus we have $\mathcal{H}_3 \subseteq \mathcal{H}_2$. \square

B.2 The Derivation of the ELBO

We use q to represent $q(s_{1:T} \mid o_{1:T}, a_{1:T}, r_{1:T})$, \hat{q} to present $q(s_t \mid o_{\leq t}, a_{< t}, r_{< t})$, \tilde{q} to represent $q(s_{t-1} \mid o_{\leq (t-1)}, r_{< (t-1)}, a_{< (t-1)})$, and we have

$$\begin{aligned} &\ln p(o_{1:T}, r_{1:T}, \mathcal{M} \mid a_{1:T}) \\ &= \ln \mathbb{E}_{p(s_{1:T} \mid a_{1:T})} [p(o_{1:T}, r_{1:T}, \mathcal{M} \mid s_{1:T})] \\ &= \ln \mathbb{E}_{p(s_{1:T} \mid a_{1:T})} [p(o_{1:T}, r_{1:T} \mid \mathcal{M}, s_{1:T}) p(\mathcal{M} \mid s_{1:T})] \\ &= \ln \mathbb{E}_{p(s_{1:T} \mid a_{1:T})} \left[p(\mathcal{M} \mid s_{1:T}) \prod_{t=1}^T p(o_t, r_t \mid \mathcal{M}, s_t) \right] \\ &= \ln \mathbb{E}_q \left[p(\mathcal{M} \mid s_{1:T}) \prod_{t=1}^T p(o_t, r_t \mid \mathcal{M}, s_t) \frac{p(s_t \mid s_{t-1}, a_{t-1})}{q(s_t \mid o_{\leq t}, r_{< t}, a_{< t})} \right] \\ &\geq \mathbb{E}_q [\ln p(\mathcal{M} \mid s_{1:T}) + \sum_{t=1}^T \ln p(o_t, r_t \mid \mathcal{M}, s_t)] \\ &+ \mathbb{E}_q \sum_{t=1}^T [\ln p(s_t \mid s_{t-1}, a_{t-1}) - \ln q(s_t \mid o_{\leq t}, r_{< t}, a_{< t})] \\ &= \mathbb{E}_q [\ln p(\mathcal{M} \mid s_{1:T})] \\ &+ \sum_{t=1}^T \left[\mathbb{E}_q \ln p(o_t, r_t \mid \mathcal{M}, s_t) - \mathbb{E}_q \ln \frac{q(s_t \mid o_{\leq t}, r_{< t}, a_{< t})}{p(s_t \mid s_{t-1}, a_{t-1})} \right] \\ &= \mathbb{E}_q [\ln p(\mathcal{M} \mid s_{1:T})] + \sum_{t=1}^T \mathbb{E}_{\tilde{q}} [\ln p(o_t, r_t \mid \mathcal{M}, s_t)] \\ &- \sum_{t=1}^T \mathbb{E}_{\hat{q}\tilde{q}} \left[\ln \frac{q(s_t \mid o_{\leq t}, r_{< t}, a_{< t})}{p(s_t \mid s_{t-1}, a_{t-1})} \right] \\ &= \mathbb{E}_q [\ln p(\mathcal{M} \mid s_{1:T})] + \sum_{t=1}^T \mathbb{E}_{\tilde{q}} [\ln p(o_t, r_t \mid \mathcal{M}, s_t)] \\ &- \sum_{t=1}^T \mathbb{E}_{\tilde{q}} [\text{KL}(q(s_t \mid o_{\leq t}, r_{< t}, a_{< t}) \parallel p(s_t \mid s_{t-1}, a_{t-1}))]. \end{aligned} \quad (11)$$

Thus we have proven the ELBO.

B.3 The Proof of Theorem 2

Proof. We first prove that for $\forall \pi \in \Pi_2$, we have $\mathbb{E}_{\mathcal{M} \sim \mathcal{T}} [J_{\mathcal{M}}(\pi)] = J_{\bar{\mathcal{M}}}(\pi)$.

For any $\mathcal{M} = (\mathcal{S}, \mathcal{A}, \mathcal{P}, \mathcal{R}_{\mathcal{M}}, \gamma) \sim \mathcal{T}$, we can use the policy π to interact with \mathcal{M} and get the trajectory $\tau = (s_0^{\mathcal{M}}, a_0^{\mathcal{M}}, r_1^{\mathcal{M}}, s_1^{\mathcal{M}}, a_1^{\mathcal{M}}, r_2^{\mathcal{M}}, \dots)$. Since the dynamic transition \mathcal{P} is the same for all \mathcal{M} and the policy $\pi \in \Pi_2$ only depends on historical states and actions, we naturally have that the distribution of all states and actions $(s_0^{\mathcal{M}}, a_0^{\mathcal{M}}, s_1^{\mathcal{M}}, a_1^{\mathcal{M}}, \dots)$ are the same for all $\mathcal{M} \sim \mathcal{T}$ as well

Algorithm 2 Task Aware Dreamer (TAD)

Require: M training tasks $\{\mathcal{M}_m\}_{m=1}^M$, M replay buffers $\{\mathcal{D}_m\}_{m=1}^M$, N testing tasks $\{\mathcal{M}_{M+n}\}_{n=1}^N$, initialize neural network parameters of world models, the policy, and the critic

- 1: **while** not converge **do**
- 2: // *Model Training*
- 3: **for** update step = 1, 2, ..., U **do**
- 4: Sample observation-action-reward pairs from each replay buffer $\{(o_t^i, a_t^i, r_t^i)_{t=1}^T\} \sim \mathcal{D}_i, i = 1, 2, \dots, M$
- 5: Calculate the deterministic state h and further calculate model states s .
- 6: Update the world models via optimizing Eq. (6).
- 7: Collect imagined trajectories from each s_t via the policy and the world models.
- 8: Use these imagined trajectories to update the policy and the critic.
- 9: **end for**
- 10: // *Data Collection*
- 11: **for** $m = 1, 2, \dots, M$ **do**
- 12: $o_1 \leftarrow \mathcal{M}_m.reset()$
- 13: **for** sample step = 1, 2, ..., S **do**
- 14: Compute h_t, s_t and sample action a_t via the policy.
- 15: $r_t, o_{t+1} \leftarrow \mathcal{M}_m.step(a_t)$
- 16: **end for**
- 17: Add these data to the replay buffer \mathcal{D}_m .
- 18: **end for**
- 19: **end while**
- 20: // *Model Evaluation*
- 21: **for** $n = 1, 2, \dots, N$ **do**
- 22: $o_1 \leftarrow \mathcal{M}_{M+n}.reset()$
- 23: **while** the environment not done **do**
- 24: Compute h_t, s_t and sample action a_t via the policy.
- 25: $r_t, o_{t+1} \leftarrow \mathcal{M}_{M+n}.step(a_t)$
- 26: **end while**
- 27: **end for**

as $\bar{\mathcal{M}}$. Consequently, we have

$$\begin{aligned} & \mathbb{E}_{\mathcal{M} \sim \mathcal{T}}[J_{\mathcal{M}}(\pi)] \\ &= \mathbb{E}_{\mathcal{M} \sim \mathcal{T}} \mathbb{E}_{\tau \sim \mathcal{P}, \pi}[\mathcal{R}_{\mathcal{M}}(\tau)] = \mathbb{E}_{\mathcal{M} \sim \mathcal{T}} \mathbb{E}_{\tau \sim \mathcal{P}, \pi} \left[\sum_{t=0}^{\infty} \gamma^t r_t^{\mathcal{M}} \right] \\ &= \mathbb{E}_{\tau \sim \mathcal{P}, \pi} \left[\sum_{t=0}^{\infty} \gamma^t \mathbb{E}_{\mathcal{M} \sim \mathcal{T}}[r_t^{\mathcal{M}}] \right] \\ &= \mathbb{E}_{\tau \sim \mathcal{P}, \pi} \left[\sum_{t=0}^{\infty} \gamma^t \mathbb{E}_{\mathcal{M} \sim \mathcal{T}}[\mathcal{R}_{\mathcal{M}}(s_t^{\mathcal{M}}, a_t^{\mathcal{M}})] \right] \\ &= \mathbb{E}_{\tau \sim \mathcal{P}, \pi} \left[\sum_{t=0}^{\infty} \gamma^t [\bar{\mathcal{R}}(s_t^{\mathcal{M}}, a_t^{\mathcal{M}})] \right] \\ &= \mathbb{E}_{\tau \sim \mathcal{P}, \pi}[\mathcal{R}_{\bar{\mathcal{M}}}(\tau)] = J_{\bar{\mathcal{M}}}(\pi). \end{aligned} \tag{12}$$

It is well known that the optimal policy in single MDP is memory-less, i.e., $\max_{\pi \in \Pi_2} J_{\bar{\mathcal{M}}}(\pi) = \max_{\pi \in \Pi_1} J_{\bar{\mathcal{M}}}(\pi)$. Consequently, we have

$$\begin{aligned} J_{\mathcal{T}}^2 &= \max_{\pi \in \Pi_2} \mathbb{E}_{\mathcal{M} \sim \mathcal{T}}[J_{\mathcal{M}}(\pi)] = \max_{\pi \in \Pi_2} J_{\bar{\mathcal{M}}}(\pi) \\ &= \max_{\pi \in \Pi_1} J_{\bar{\mathcal{M}}}(\pi) = \max_{\pi \in \Pi_1} \mathbb{E}_{\mathcal{M} \sim \mathcal{T}}[J_{\mathcal{M}}(\pi)] = J_{\mathcal{T}}^1 \tag{13} \\ &\leq \mathbb{E}_{\mathcal{M} \sim \mathcal{T}} \left[\max_{\pi \in \Pi_1} J_{\mathcal{M}}(\pi) \right] = J_{\mathcal{T}}^*. \end{aligned}$$

Thus we have proven this result. \square

B.4 The Proof of Theorem 3

Proof. Our proof follows some previous work [Kakade and Langford, 2002; Ying *et al.*, 2022]. First, we consider the bellman equation of value function of $\pi, \pi_{\mathcal{M}}^* \in \Pi_1$ in \mathcal{M} as

$$\begin{aligned} V_{\mathcal{M}, \pi}(s) &= \sum_a \pi(a|s) \left[\mathcal{R}(s, a) + \gamma \sum_{s'} \mathcal{P}(s'|s, a) V_{\mathcal{M}, \pi}(s') \right], \\ V_{\mathcal{M}, \pi_{\mathcal{M}}^*}(s) &= \sum_a \pi_{\mathcal{M}}^*(a|s) \left[\mathcal{R}(s, a) + \gamma \sum_{s'} \mathcal{P}(s'|s, a) V_{\mathcal{M}, \pi_{\mathcal{M}}^*}(s') \right]. \end{aligned}$$

Defining $\Delta V(s) \triangleq V_{\mathcal{M}, \pi}(s) - V_{\mathcal{M}, \pi_{\mathcal{M}}^*}(s)$ as the difference of these two value functions, we can further deduce that

$$\begin{aligned} & V_{\mathcal{M}, \pi}(s) - V_{\mathcal{M}, \pi_{\mathcal{M}}^*}(s) \\ &= \gamma \sum_a \Delta \pi(a|s) \sum_{s'} \mathcal{P}(s'|s, a) V_{\mathcal{M}, \pi_{\mathcal{M}}^*}(s') \\ &+ \gamma \sum_a \pi(a|s) \sum_{s'} \mathcal{P}(s'|s, a) \Delta V(s') + \sum_a \Delta \pi(a|s) \mathcal{R}(s, a) \\ &= \sum_a \Delta \pi(a|s) Q_{\mathcal{M}, \pi_{\mathcal{M}}^*}(s, a) \\ &+ \gamma \sum_a \pi(a|s) \sum_{s'} \mathcal{P}(s'|s, a) \Delta V(s'), \end{aligned} \tag{14}$$

here $\Delta\pi(a|s) = \pi(a|s) - \pi_{\mathcal{M}}^*(a|s)$. Since Eq. (14) holds for any s , thus we calculate its expectation for $s \sim d_{\mathcal{M}}^{\pi_{\mathcal{M}}^*}$:

$$\begin{aligned}
& \sum_s d_{\mathcal{M}}^{\pi}(s) \Delta V(s) \\
&= \sum_s d_{\mathcal{M}}^{\pi}(s) [V_{\mathcal{M},\pi}(s) - V_{\mathcal{M},\pi_{\mathcal{M}}^*}(s)] \\
&= \sum_s d_{\mathcal{M}}^{\pi}(s) \sum_a \Delta\pi(a|s) Q_{\mathcal{M},\pi_{\mathcal{M}}^*}(s, a) \\
&+ \gamma \sum_s d_{\mathcal{M}}^{\pi}(s) \sum_a \pi(a|s) \sum_{s'} \mathcal{P}(s'|s, a) \Delta V(s') \quad (15) \\
&= \sum_s d_{\mathcal{M}}^{\pi}(s) \sum_a \Delta\pi(a|s) Q_{\mathcal{M},\pi_{\mathcal{M}}^*}(s, a) \\
&+ \sum_{s'} \Delta V(s') \left[\gamma \sum_s d_{\mathcal{M}}^{\pi}(s) \sum_a \pi(a|s) \mathcal{P}(s'|s, a) \right].
\end{aligned}$$

Since $\gamma \sum_{s'} d_{\mathcal{M}}^{\pi}(s') \sum_a \pi(a|s') \mathcal{P}(s|s', a) = d_{\mathcal{M}}^{\pi}(s) - (1 - \gamma) \mathcal{P}(s_0 = s)$, we have

$$\begin{aligned}
\sum_s d_{\mathcal{M}}^{\pi}(s) \Delta V(s) &= \sum_s d_{\mathcal{M}}^{\pi}(s) \sum_a \Delta\pi(a|s) Q_{\mathcal{M},\pi_{\mathcal{M}}^*}(s, a) \\
&+ \sum_{s'} \Delta V(s') [d_{\mathcal{M}}^{\pi}(s') - (1 - \gamma) \mathcal{P}(s_0 = s')]. \quad (16)
\end{aligned}$$

By moving the second term of the right part in Eq. (16) to the left part, we can deduce that

$$\begin{aligned}
& (1 - \gamma) \sum_{s'} \Delta V(s') \mathcal{P}(s_0 = s') \\
&= \sum_s d_{\mathcal{M}}^{\pi}(s) \sum_a \Delta\pi(a|s) Q_{\mathcal{M},\pi_{\mathcal{M}}^*}(s, a), \quad (17)
\end{aligned}$$

thus we can calculate that

$$\begin{aligned}
& J_{\mathcal{M}}(\pi) - J_{\mathcal{M}}(\pi_{\mathcal{M}}^*) = \sum_{s'} \Delta V(s') \mathcal{P}(s_0 = s') \\
&= \frac{1}{1 - \gamma} \sum_s d_{\mathcal{M}}^{\pi}(s) \sum_a \Delta\pi(a|s) Q_{\mathcal{M},\pi_{\mathcal{M}}^*}(s, a) \\
&= \frac{1}{1 - \gamma} \sum_s d_{\mathcal{M}}^{\pi}(s) \sum_a [\pi(a|s) - \pi_{\mathcal{M}}^*(a|s)] Q_{\mathcal{M},\pi_{\mathcal{M}}^*}(s, a) \\
&= \frac{1}{1 - \gamma} \mathbb{E}_{s \sim d_{\mathcal{M}}^{\pi}} \mathbb{E}_{a \sim \pi(\cdot|s)} \left(1 - \frac{\pi_{\mathcal{M}}^*(a|s)}{\pi(a|s)} \right) Q_{\mathcal{M},\pi_{\mathcal{M}}^*}(s, a) \\
&= \frac{1}{1 - \gamma} \mathbb{E}_{s \sim d_{\mathcal{M}}^{\pi}} \int_{\mathcal{A}} \pi(a|s) \left(1 - \frac{\pi_{\mathcal{M}}^*(a|s)}{\pi(a|s)} \right) Q_{\mathcal{M}}^*(s, a) da \\
&= \frac{1}{1 - \gamma} \mathbb{E}_{s \sim d_{\mathcal{M}}^{\pi}} \left[\int_a \pi(a|s) Q_{\mathcal{M}}^*(s, a) da - \max_a Q_{\mathcal{M}}^*(s, a) \right]. \quad (18)
\end{aligned}$$

Consequently, we have

$$\begin{aligned}
& \mathbb{E}_{\mathcal{M} \sim \mathcal{T}} [J_{\mathcal{M}}(\pi_{\mathcal{M}}^*) - J_{\mathcal{M}}(\pi)] \\
&= \frac{1}{1 - \gamma} \mathbb{E}_{\mathcal{M} \sim \mathcal{T}} \mathbb{E}_{s \sim d_{\mathcal{M},\pi}(\cdot)} \left[\max_a Q_{\mathcal{M}}^*(s, a) \right. \\
&\quad \left. - \int_a \pi(a|s) Q_{\mathcal{M}}^*(s, a) da \right] \\
&\geq \frac{1}{1 - \gamma} \mathbb{E}_{s \sim d_{\mathcal{M},\pi}(\cdot)} \left[\mathbb{E}_{\mathcal{M} \sim \mathcal{T}} \max_a Q_{\mathcal{M}}^*(s, a) \right. \\
&\quad \left. - \max_a \mathbb{E}_{\mathcal{M} \sim \mathcal{T}} Q_{\mathcal{M}}^*(s, a) \right] \\
&= \frac{1}{1 - \gamma} \mathbb{E}_{s \sim d_{\mathcal{M},\pi}} [D_{\text{TDR}}(\mathcal{T}, s)]. \quad (19)
\end{aligned}$$

Since $J_{\mathcal{M}}(\pi_{\mathcal{M}}^*) = \max_{\pi \in \Pi_1} J_{\mathcal{M}}(\pi)$, we have

$$\begin{aligned}
& \mathbb{E}_{\mathcal{M} \sim \mathcal{T}} \max_{\pi \in \Pi_1} J_{\mathcal{M}}(\pi) - \max_{\pi \in \Pi_1} \mathbb{E}_{\mathcal{M} \sim \mathcal{T}} J_{\mathcal{M}}(\pi) \\
&\geq \frac{1}{1 - \gamma} \mathbb{E}_{s \sim d_{\mathcal{M},\pi^*}} [D_{\text{TDR}}(\mathcal{T}, s)], \quad (20)
\end{aligned}$$

Thus we have proven this result. \square

B.5 Expressive Ability of Π_3

Proposition 1. For $\forall \epsilon_1, \epsilon_2$ satisfying $0 < \epsilon_1 \leq 1, 0 < \epsilon_2 \leq 1$, there exists a task distribution \mathcal{T} satisfying that

$$J_{\mathcal{T}}^1 = J_{\mathcal{T}}^2 \leq \epsilon_1, \quad J_{\mathcal{T}}^3 \geq 1 - \epsilon_2, \quad J_{\mathcal{T}}^* = 1. \quad (21)$$

Proof. Given fixed discount factor $\gamma \in (0, 1)$, we first take $n \in \mathbb{N}$ satisfying $n \geq \frac{1}{\epsilon_1}$, $A = \epsilon_2 \frac{n}{n-1} \frac{1-\gamma}{1-\gamma^n}$, and $B = \frac{1-\gamma}{\gamma^{n+1}} \left(1 - \epsilon_2 \frac{n}{n-1} \right)$. We construct state sets $\mathcal{S} = \{s_t^l\} (t = 0, 1, \dots, \infty, l = 1, \dots, n)$ and action sets $\mathcal{A} = \{a_j\}_{j=1}^n$. Then we construct n tasks $\mathcal{M}_i = (\mathcal{S}, \mathcal{A}, \mathcal{P}, \mathcal{R}_i, \gamma), i = 1, \dots, n$, which share the same dynamic \mathcal{P} and different reward functions \mathcal{R}_i . The initial state of each task is s_0^1 , and the dynamic as well as reward functions are as below

$$\begin{aligned}
& \mathcal{P}(s_t^l, a_j) = \mathbb{I}(s = s_{t+1}^j), \quad j, l = 1, \dots, n; t = 0, 1, \dots, \infty \\
& \mathcal{R}_i(s_t^l, a_j) = f(t) \mathbb{I}(i = j), \quad i, j, l = 1, \dots, n; t = 0, 1, \dots, \infty \\
& f(t) = \begin{cases} A, & t \leq n-1 \\ B, & t \geq n \end{cases} \quad (22)
\end{aligned}$$

Take \mathcal{T} as the uniform distribution over $\mathcal{M}_1, \dots, \mathcal{M}_n$, thus we have

$$\begin{aligned}
& J_{\mathcal{M}_i}^* = A + A\gamma + \dots + A\gamma^{n-1} + B\gamma^n + B\gamma^{n+1} + \dots \\
& = A \frac{1 - \gamma^n}{1 - \gamma} + B \frac{\gamma^{n+1}}{1 - \gamma} = 1 \quad (23)
\end{aligned}$$

$$J_{\mathcal{T}}^* = \frac{1}{n} \sum_{i=1}^n J_{\mathcal{M}_i}^* = 1.$$

Since our construction satisfies $\mathbb{E}_{\mathcal{T}}[\mathcal{R}_i(s_k^l, a_j)] = \frac{f(k)}{n}$, for

$\forall \pi \in \Pi_2$, we have

$$\begin{aligned} J_{\mathcal{T}}(\pi) &= \frac{1}{n}(A + A\gamma + \dots + A\gamma^{n-1} + B\gamma^n + B\gamma^{n+1} + \dots) \\ &= \frac{1}{n}, \\ J_{\mathcal{T}}^1 &= J_{\mathcal{T}}^2 = \max_{\pi \in \Pi_2} J_{\mathcal{T}}(\pi) = \frac{1}{n} \leq \epsilon_1. \end{aligned} \quad (24)$$

Moreover, we can construction an agent $\hat{\pi} \in \Pi_3$ that takes action via the historical trajectory $\hat{\tau}_t = (\hat{s}_0, \hat{a}_0, \hat{r}_0, \dots, \hat{s}_t)$:

$$\begin{aligned} \hat{\pi}(a_j | \hat{\tau}_t) &= \mathbb{I}(j = t + 1), \quad t = 0, 1, \dots, n - 1 \\ \hat{\pi}(a_j | \hat{\tau}_t) &= \mathbb{I}(j = i), \quad t = n, \dots, \infty \end{aligned} \quad (25)$$

here $i = \arg \max\{\hat{r}_0, \hat{r}_1, \dots, \hat{r}_{n-1}\} + 1$, thus we have

$$\begin{aligned} J_{\mathcal{T}}^3 &\geq J_{\mathcal{T}}(\hat{\pi}) \\ &= \frac{1}{n}(A + A\gamma + \dots + A\gamma^{n-1}) + B\gamma^n + B\gamma^{n+1} + \dots \\ &= \frac{A}{n} \frac{1 - \gamma^n}{1 - \gamma} + B \frac{\gamma^{n+1}}{1 - \gamma} = 1 - \frac{(n-1)A}{n} \frac{1 - \gamma^n}{1 - \gamma} \\ &\geq 1 - \epsilon_2. \end{aligned} \quad (26)$$

Thus we have proven this result. \square

B.6 Proof and Discussion of Theorem 4

In this part, we introduce an informed version of Theorem 4, about why optimizing $p(\mathcal{M}|l) \forall l \in \mathcal{L}$ is beneficial for task generalization, with detailed proofs. Recall that we consider the policy hypothesis \mathcal{H}_3 here, that each policy $\pi : \mathcal{L} \rightarrow \Delta(\mathcal{A})$, $\mathcal{L} = \cup_{t=1}^{\infty} \mathcal{L}_t$, $\mathcal{L}_t = (\mathcal{S} \times \mathcal{A} \times \mathbb{R})^{t-1} \times \mathcal{S}$. As directly such $\mathcal{S} - \mathcal{A} - \mathcal{R}$ memorized policy is difficult, we consider an alternative MDP as $\tilde{\mathcal{M}} = (\tilde{\mathcal{L}}, \mathcal{A}, \mathcal{P}_{\mathcal{M}}, \mathcal{R}_{\mathcal{M}}, \gamma)$. For $\forall l = (s_1, a_1, r_1, \dots, s_t) \in \mathcal{L}_t \subseteq \mathcal{L}$, we can sample the action a_t from the distribution $\pi(\cdot|l)$. Then the environment will feedback the reward signal $r_t = \mathcal{R}_{\mathcal{M}}(l, a_t) = \mathcal{R}_{\mathcal{M}}(s_t, a_t)$, we can sample s_{t+1} from the distribution $\mathcal{P}(\cdot|s_t, a_t)$, and the next environment state will be $l' = (s_1, a_1, r_1, \dots, s_t, a_t, r_t, s_{t+1}) \in \mathcal{L}_{t+1}$. In summary, we set the distribution $p(l'|l, a_t)$ as the corresponding dynamic $\mathcal{P}_{\mathcal{M}}$. Notice that although all $\mathcal{M} \in \mathcal{T}$ shares the same dynamic \mathcal{P} , their new dynamic $\mathcal{P}_{\mathcal{M}}$ are different since the dynamic is related to the given reward. An obvious advantage of introducing $\tilde{\mathcal{M}}$ is that $\pi \in \Pi_3$ is now Markovian in $\tilde{\mathcal{M}}$ and it is much easier to analyze its performance.

Obviously, we can set $J_{\mathcal{M}}(\pi) = J_{\tilde{\mathcal{M}}}(\pi)$, $Q_{\mathcal{M}}^*(s, a) = Q_{\tilde{\mathcal{M}}}^*(s, a)$ to simplify the notation, and we can prove that

Theorem 6. For any policy $\pi \in \Pi_3$, we have

$$\begin{aligned} &J_{\mathcal{T}}^* - \mathbb{E}_{\mathcal{M} \sim \mathcal{T}} [J_{\mathcal{M}}(\pi)] \\ &= \frac{1}{1 - \gamma} \int_{\mathcal{L}} p(l) \left[\int p(\mathcal{M}|l) \max_a Q_{\mathcal{M}}^*(l, a) d\mathcal{M} \right. \\ &\quad \left. - \int_{a, \mathcal{M}} \pi(a|l) p(\mathcal{M}|l) Q_{\mathcal{M}}^*(l, a) da d\mathcal{M} \right] dl \\ &\geq \frac{1}{1 - \gamma} \int_{\mathcal{L}} p(l) \left[\int p(\mathcal{M}|l) \max_a Q_{\mathcal{M}}^*(l, a) d\mathcal{M} \right. \\ &\quad \left. - \max_a \int_{\mathcal{M}} p(\mathcal{M}|l) Q_{\mathcal{M}}^*(l, a) d\mathcal{M} \right] dl, \end{aligned} \quad (27)$$

here $p(l)$ is a distribution of \mathcal{L} related to \mathcal{T} , π and $p(\mathcal{M}|l)$ is the task posterior related to π .

Proof. $\forall \pi \in \mathcal{H}_3$, as π is Markovian in $\tilde{\mathcal{M}}$, we can directly utilize the proof of Theorem 3 from the beginning to Eq. (18), and the only difference is that the dynamics in $\tilde{\mathcal{M}}$ are different but the dynamics in \mathcal{M} are the same. Thus we need to change the Eq. (19) as

$$\begin{aligned} &\mathbb{E}_{\mathcal{M} \sim \mathcal{T}} [J_{\mathcal{M}}(\pi_{\mathcal{M}}^*) - J_{\mathcal{M}}(\pi)] \\ &= \frac{1}{1 - \gamma} \mathbb{E}_{\mathcal{M} \sim \mathcal{T}} \mathbb{E}_{l \sim d_{\tilde{\mathcal{M}}, \pi}(\cdot)} \left[\max_a Q_{\mathcal{M}}^*(l, a) \right. \\ &\quad \left. - \int_a \pi(a|l) Q_{\mathcal{M}}^*(l, a) da \right] \\ &= \frac{1}{1 - \gamma} \int p(\mathcal{M}) \int_{\mathcal{L}} d_{\tilde{\mathcal{M}}, \pi}(l) \left[\max_a Q_{\mathcal{M}}^*(l, a) \right. \\ &\quad \left. - \int_a \pi(a|l) Q_{\mathcal{M}}^*(l, a) da \right] \\ &= \frac{1}{1 - \gamma} \int_{\mathcal{L}} p(l) \int p(\mathcal{M}|l) \left[\max_a Q_{\mathcal{M}}^*(l, a) \right. \\ &\quad \left. - \int_a \pi(a|l) Q_{\mathcal{M}}^*(l, a) da \right] \\ &\geq \frac{1}{1 - \gamma} \int_{\mathcal{L}} p(l) \left[\int p(\mathcal{M}|l) \max_a Q_{\mathcal{M}}^*(l, a) d\mathcal{M} \right. \\ &\quad \left. - \max_a \int_{\mathcal{M}} Q_{\mathcal{M}}^*(l, a) d\mathcal{M} \right] dl, \end{aligned} \quad (28)$$

here $p(l) = \int p(\mathcal{M}) d_{\tilde{\mathcal{M}}, \pi}(l) d\mathcal{M}$, and $p(\mathcal{M}|l) = p(\mathcal{M}) d_{\tilde{\mathcal{M}}, \pi}(l) / p(l)$ is the posterior distribution. \square

Finally, we will show that maximizing $p(\mathcal{M}|l)$ is helpful for task generalization. In the training stage, we will sample a task \mathcal{M} and corresponding state-action-reward pairs l , thus optimizing $p(\mathcal{M}|l)$ will make it to be closer to some Dirac distribution. In such a situation, for each l , we can infer a “most possible” posterior task \mathcal{M}_l with high $p(\mathcal{M}_l|l)$, thus we can approximately take $\pi(l) = \arg \max_a Q_{\mathcal{M}_l}^*(l, a)$ and the optimal gap calculated by E.q. (27) will be controlled.

B.7 Sparse Reward Task

In this part, we show that generalizing to tasks with the same dynamics and sparse rewards without extra knowledge (like context) is extremely difficult and sometimes impossible. It is because we cannot distinguish them via historical information. Here we construct an example.

Assume there are n MDPs, $\mathcal{M}_i (i = 1, \dots, n)$, each MDP share the same state set $\mathcal{S} = \{s_1, \dots, s_T\}$ and action set $\mathcal{A} = \{a_1, \dots, a_n\}$. The initial state is s_1 and the dynamic is that $\mathcal{P}(s_{t+1}|s_t, a_i) = 1 (t = 1, \dots, T - 1, i = 1, \dots, n)$, $\mathcal{P}(s_T|s_T, a_i) = 1 (i = 1, \dots, n)$. As for the reward function, we define that

$$\mathcal{R}_{\mathcal{M}_i}(s_{T-1}, a_i) = 1, i = 1, \dots, n. \quad (29)$$

and the reward function is 0 otherwise. In this case, any policies (including markovian, state-action memorized, and state-action-reward memorized) in this task distribution can only handle one task since they can not distinguish them.

C Experimental Details for DMControl

C.1 Details of All Task Combinations

In this part, we first *roughly* discuss the reward function of tasks in our experiments to better understand their TDR. These reward functions always defined by tolerance function in DeepMind control suite [Tassa *et al.*, 2018], which is a smooth function with parameters $\text{tolerance}(x, \text{bounds} = (\text{lower}, \text{upper}))$ and hope the value of x is within $(\text{lower}, \text{upper})$. More details about tolerance function can be found in [Tassa *et al.*, 2018].

- **Walker-stand&walk.** This task combination includes two tasks: Walker-stand and Walker-walk, which both require a two-leg robot to maintain its height above a certain threshold, and Walker-walk also hopes it to move faster than a certain speed, i.e., their reward functions can be roughly described as

$$\begin{aligned}\mathcal{R}_{\text{stand}} &= \text{tolerance}(\text{height}, (1.2, \infty)), \\ \mathcal{R}_{\text{walk}} &= \text{tolerance}(\text{height}, (1.2, \infty)) \\ &\quad * \text{tolerance}(\text{speed}, (1, \infty)).\end{aligned}\quad (30)$$

Therefore, for all states, the optimal action of Walker-walk is also optimal in Walker-stand and TDR here is 0.

- **Cartpole-balance&sparse.** This task combination includes two tasks: Cartpole-balance and Cartpole-balance_sparse, which both hope to balance an unactuated pole with dense and sparse rewards respectively. The optimal actions of these tasks are both hope to balance the agent and thus TDR here is 0.
- **Acrobot-swingup&sparse.** This task combination includes two tasks: Acrobot-swingup and Acrobot-swingup_sparse, which both hope to swing up a double pendulum with dense and sparse rewards respectively. Also, the optimal actions of these tasks are both hoped to swingup the agent and thus TDR here is 0.
- **Quadruped-walk&run.** This task combination includes two tasks: Quadruped-walk and Quadruped-run, which both require a quadruped agent to move faster than a target speed. The target speed of the running task is larger than the walking task, i.e., their reward functions can be roughly described as

$$\begin{aligned}\mathcal{R}_{\text{walk}} &= \text{tolerance}(\text{speed}, (0.5, \infty)), \\ \mathcal{R}_{\text{run}} &= \text{tolerance}(\text{speed}, (5.0, \infty)).\end{aligned}\quad (31)$$

Therefore, TDR here is still 0 since optimal actions of Quadruped-run are also optimal in Quadruped-walk.

- **Reacher-easy&hard.** This task combination includes two tasks: Reacher-easy and Reacher-hard, which both hope to control a two-link planar reacher to prostrate the target sphere. The sizes of target spheres in these two tasks are different, i.e., their reward functions can be roughly described as

$$\begin{aligned}\mathcal{R}_{\text{easy}} &= \text{tolerance}(\text{distance}, (0.0, 0.05)), \\ \mathcal{R}_{\text{hard}} &= \text{tolerance}(\text{distance}, (0.0, 0.015)).\end{aligned}\quad (32)$$

Thus TDR here is not 0 but still small.

- **Hopper-stand&hop.** This task combination includes two tasks: Hopper-stand and Hopper-hop, which both hope the height of a one-legged hopper is larger than the target height. While Hopper-stand hopes the control force is 0, Hopper-hop hopes to control the robot to hop forward and its speed is larger than the target speed. Their reward functions can be roughly described as

$$\begin{aligned}\mathcal{R}_{\text{stand}} &= \text{tolerance}(\text{height}, (0.6, 2)) \\ &\quad * \text{tolerance}(\text{speed}, (2.0, \infty)), \\ \mathcal{R}_{\text{hop}} &= \text{tolerance}(\text{height}, (0.6, 2)) \\ &\quad * \text{tolerance}(\text{control}, (0.0, 0.0)).\end{aligned}\quad (33)$$

Since one agent can not hop when controlling the force as 0, TDR here is not 0 but not huge.

- **Walker-stand&prostrate.** This task combination includes two tasks: Walker-stand and Walker-prostrate. Walker-stand hopes the height of a two-leg robot to be larger than the target height. And we design the task Walker-prostrate, which hopes its height to be lower than another target height. Their reward functions can be roughly described as

$$\begin{aligned}\mathcal{R}_{\text{stand}} &= \text{tolerance}(\text{height}, (1.2, \infty)), \\ \mathcal{R}_{\text{prostrate}} &= \text{tolerance}(\text{height}, (0.0, 0.2)).\end{aligned}\quad (34)$$

Thus TDR here is huge since the optimal Q functions of these two tasks are almost the opposite.

- **Walker-walk&prostrate.** This task combination includes two tasks: Walker-walk and Walker-prostrate. Walker-walk hopes the height of the improved planar walker to be larger than a target height, while Walker-prostrate hopes it to be lower than a target height. Moreover, Walker-walk hopes the speed of the robot is larger than another target speed, i.e., their reward functions can be roughly described as

$$\begin{aligned}\mathcal{R}_{\text{walk}} &= \text{tolerance}(\text{height}, (1.2, \infty)) \\ &\quad * \text{tolerance}(\text{speed}, (1.0, \infty)), \\ \mathcal{R}_{\text{prostrate}} &= \text{tolerance}(\text{height}, (0.0, 0.2)).\end{aligned}\quad (35)$$

Thus TDR here is also huge since the optimal Q functions of these two tasks are almost the opposite.

C.2 Details of All Task Distributions

Now we introduce the three task distributions in our experiments, which are designed based on existing tasks in DeepMind control suite for testing the generalization of trained agents.

- **Cheetah_speed(α, β).** This task distribution is designed in this paper with parameter $0 \leq \beta \leq \alpha$, based on the task Cheetah_run in DeepMind control suite, and hopes the Cheetah robot can run with the target speed interval $(\alpha - \beta, \alpha + \beta)$.

$$\mathcal{R}_{\text{Cheetah_speed}}(\alpha, \beta) = \text{tolerance}(\text{speed}, (\alpha - \beta, \alpha + \beta)).\quad (36)$$

We train the agents in tasks with parameters (0.5, 0.2), (1.5, 0.2), (2.0, 0.2), (3.0, 0.2) and test them in tasks with parameters (1.0, 0.2), (2, 5, 0.2).

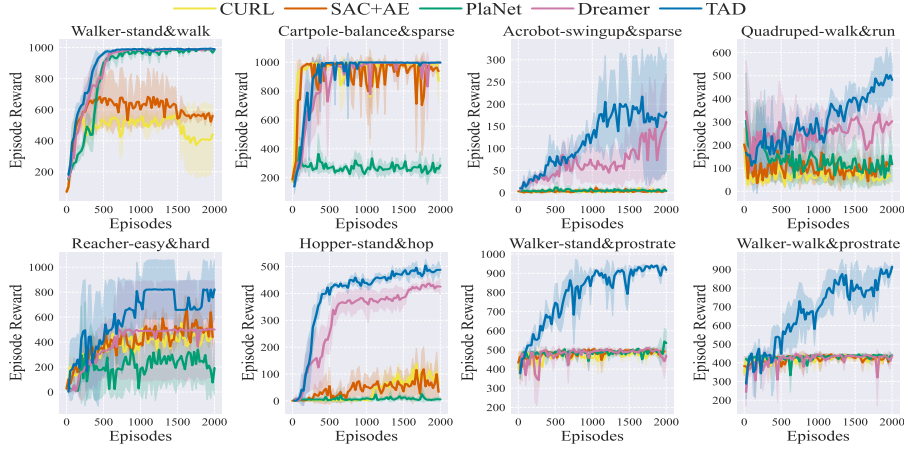


Figure 4: Average cumulative reward curves over different task combinations in DMC for CURL, SAC+AE, PlaNet, Dreamer, and TAD. The x-axes indicate the number of episodes interacting with the environment, and the y-axes indicate the performance, including average rewards with std.

Tasks	Hypothesis	Walker-stand&walk	Cartpole-balance&sparse	Acrobot-swingup&sparse	Quadruped-walk&run
CURL	Π_1	563.4 ± 16.0	996.8 ± 0.8	11.0 ± 1.8	203.3 ± 69.9
SAC+AE	Π_1	683.8 ± 164.3	993.4 ± 0.6	11.7 ± 5.4	203.2 ± 70.2
PlaNet	Π_2	990.6 ± 3.8	412.8 ± 65.9	12.2 ± 9.8	305.3 ± 206.6
Dreamer	Π_2	992.3 ± 1.7	997.1 ± 1.1	159.9 ± 108.4	345.4 ± 218.3
TAD	Π_3	993.9 ± 1.0	998.9 ± 0.3	217.3 ± 107.1	505.0 ± 119.1
Tasks	Hypothesis	Reacher-easy&hard	Hopper-stand&hop	Walker-stand&prostrate	Walker-walk&prostrate
CURL	Π_1	552.5 ± 88.9	137.1 ± 9.2	496.3 ± 8.7	441.0 ± 7.7
SAC+AE	Π_1	669.5 ± 99.4	118.2 ± 83.1	504.4 ± 6.7	445.8 ± 2.6
PlaNet	Π_2	341.0 ± 228.3	25.9 ± 25.7	544.3 ± 68.6	445.4 ± 5.1
Dreamer	Π_2	506.1 ± 382.9	436.9 ± 18.9	510.0 ± 6.7	449.7 ± 12.5
TAD	Π_3	823.3 ± 237.4	503.9 ± 22.2	941.1 ± 4.0	913.7 ± 11.5

Table 5: Performance (mean \pm std) over different task combinations in image-based DMC of the best policy. Numbers greater than **95** % of the best performance for each environment are **bold**.

- **Pendulum_angle**(α, β). This task distribution is designed in this paper with parameter $-1 \leq \alpha \leq \beta \leq 1$, based on the task Pendulumh_swingup in DeepMind control suite, and hopes the Pendulum robot can swing up within the target angle interval ($\arccos \alpha, \arccos \beta$).

$$\mathcal{R}_{\text{Pendulum_angle}}(\alpha, \beta) = \text{tolerance}(\text{angle}, (\arccos \alpha, \arccos \beta)). \quad (37)$$

Training tasks are with parameters $(-0.95, -0.9)$, $(-0.85, -0.8)$, $(-0.8, -0.75)$, $(-0.7, -0.65)$ and testing tasks are with parameters $(-0.9, -0.85)$, $(-0.75, -0.7)$.

- **Walker_speed**(α, β). This task distribution is designed in this paper with parameter $0 \leq \beta \leq \alpha$, based on the task Walker_run in DeepMind control suite, and hopes the Walker robot can run within the target speed interval $(\alpha - \beta, \alpha + \beta)$.

$$\mathcal{R}_{\text{Walker_speed}}(\alpha, \beta) = \text{tolerance}(\text{speed}, (\alpha - \beta, \alpha + \beta)). \quad (38)$$

We train the agents in tasks with parameters $(0.5, 0.2)$,

$(1.5, 0.2)$, $(2.0, 0.2)$, $(3.0, 0.2)$ and test in tasks with parameters $(1.0, 0.2)$, $(2, 5, 0.2)$.

Moreover, we introduce some details about our experiments. Our codes are based on Python and the deep learning library PyTorch. All algorithms are trained on one NVIDIA GeForce RTX 2080 Ti. As for the hyper-parameters, we follow previous works [Ha and Schmidhuber, 2018; Hafner *et al.*, 2019b; Hafner *et al.*, 2019a] and select 2 as the action repeat for all experiments following [Hafner *et al.*, 2019a].

C.3 Full Experimental Results for TDR

In tasks where TDR is 0, like Walker-stand&walk and Cartpole-balance&sparse, the optimal performance of TAD and baselines are similar since these tasks share the same optimal action and Π_1, Π_2 own the optimal policy, as derived in Theorem 2. In these cases, TAD still converges faster and shows more robust performance. In Acrobot-swingup&sparse and Quadruped-walk&run, although TDR of these tasks is 0, TAD can surpass baselines since it can better distinguish different tasks. Finally, in the last four environments with non-zero TDR, TAD achieves a notable improvement compared with baselines. Especially, in Walker-stand&prostrate and Walker-walk&prostrate, where TDR is significantly huge,

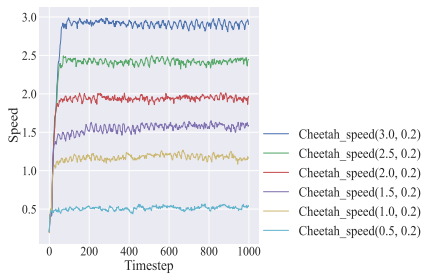


Figure 5: Visualization of the trained TAD agent in the task distribution of Cheetah_speed. We plot the speed of the agent as a function of timesteps in all tasks.

baselines perform poorly as these policies belong to Π_1, Π_2 and can not differentiate different tasks, which also aligns with our Theorem 2. In contrast, TAD can distinguish between tasks by utilizing reward signals and improves performance conspicuously.

C.4 Visualization Results for Task Generalization

Moreover, for each task sampled from the task distribution Cheetah_speed (here parameters $(3.0, 0.2)$, $(2.0, 0.2)$, $(1.5, 0.2)$, $(0.5, 0.2)$ are for training tasks and parameters $(2.5, 0.2)$, $(0.5, 0.2)$ are for testing tasks), we plot the speed of the agent as a function of the timestep in Fig. 5. As depicted, for each task, the agent trained by TAD will quickly improve its speed until reaching the target speed and then keep its speed since the speed determines whether it has met the task requirements via utilizing historical information. Consequently, TAD is aware of different tasks and can successfully generalize to unseen test tasks. We also provide videos of these trajectories in supplementary materials.

D Experimental Details for MuJoCo

We here introduce state-based control tasks (Half-CheetahFwd-Back, Half-Cheetah-Vel, and Humanoid-Direc-2D) in detail, following the setting of previous meta RL works [Finn *et al.*, 2017; Rakelly *et al.*, 2019].

- **Half-Cheetah-Fwd-Back.** This task distribution includes two tasks: moving forward and moving backward.
- **Half-Cheetah-Vel.** This task distribution hopes the agent to move forward and achieve the target velocity. There are 100 training tasks and 30 testing tasks for experiments.
- **Humanoid-Direc-2D.** This task distribution hopes the agent to move in the target direction. There are 100 training tasks and 30 testing tasks for experiments.

Moreover, we introduce some details about our experiments. Our codes are based on Python and the deep learning library PyTorch. All algorithms are trained on one NVIDIA GeForce RTX 2080 Ti. We select 1 as the action repeat for all experiments following.

E Ablation Study

E.1 Dynamic Generalization

As TAD utilizes all historical information to infer the environment, it can be directly applied to more general settings with different observations, dynamics, and/or actions. To evaluate the performance of TAD in these settings, we have conducted the following four experiments based on DMControl:

- **Acrobot-Cartpole-Pendulum:** includes 7 tasks of artpole-balance, cartpole-balance_sparse, cartpole-swingup, cartpole-swingup_sparse, acrobot-swingup, acrobot-swingup_sparse, and pendulum-swingup. All these tasks aim to control a rod-shaped robot, while they own different **embodiments**, **dynamics**, and **observations**.
- **Walker-Cheetah-Hopper:** includes 6 tasks of walker-prostrate, walker-stand, walker-walk, cheetah-run, hopper-stand, and hopper-hop. The tasks own different **embodiments**, **dynamics**, **actions**, and **observations**.
- **Cheetah-run-mass(m):** This task distribution is based on the task Cheetah-run and the mass of the robot is m times that of the standard task. Thus different tasks own different **dynamics**. We train the agents in tasks with $m = 0.6, 1.0, 1.2, 1.6$ and test them in tasks with parameters $m = 0.8, 1.4$.
- **Walker-walk-mass(m):** This task distribution is based on the task Walker-walk and the mass of the robot is m times that of the standard task. Thus different tasks own different **dynamics**. We train the agents in tasks with $m = 0.6, 1.0, 1.2, 1.6$ and test them in tasks with parameters $m = 0.8, 1.4$.

Then we test Dreamer and TAD in these four settings and report the results. TAD can achieve much greater performance and better convergence compared to Dreamer, as it can better infer the current task. This experiment indicates TAD’s potential in further handling dynamic generalization and even cross-embodiment tasks.

E.2 Sparse Reward

In this part, we will evaluate TAD in more challenging settings with sparse rewards. First, we evaluate Dreamer and TAD in Cheetah_speed with different β , which identifies the region of target speeds. With smaller β , the reward signals are more sparse since the target intervals are smaller. In the main experiment, we take $\beta = 0.2$, and here we evaluate in $\beta = 0.2, 0.15, 0.1$, of which the result is reported in Table 6. For each β , we take the training parameters $(0.5, \beta)$, $(1.5, \beta)$, $(2.0, \beta)$, $(3.0, \beta)$ and test them in tasks with parameters $(1.0, \beta)$, $(2.5, \beta)$. As shown in Table 6, with the decreasing of β , the performance of Dreamer and TAD decreases since reward signals are sparse so exploration here is much more difficult. However, our TAD still significantly outperforms Dreamer and shows strong generalization abilities, which shows that TAD can effectively utilize historical information, even sparse rewards.

Moreover, we design Cheetah_speed_sparse based on Cheetah_speed. In Cheetah_speed_sparse(n), we make the

β	0.2		0.15		0.1	
	Train	Test	Train	Test	Train	Test
Dreamer	250.2 \pm 9.6	3.0 \pm 2.2	247.5 \pm 1.0	0.0 \pm 0.0	175.8 \pm 55.8	13.5 \pm 13.5
TAD	951.9 \pm 3.3	876.9 \pm 51.1	927.6 \pm 2.6	800.1 \pm 121.4	608.5 \pm 321.4	491.6 \pm 389.4

Table 6: Average cumulative reward (mean \pm one std) over different target region (smaller β represents smaller target region and more sparse return) of the best policy trained by Dreamer and TAD in Cheetah.Speed. For each β , we train agents in the train tasks and evaluate them in both train and test environments. Numbers greater than 95 percent of the best performance for each environment are **bold**.

SR	0.0		0.8		0.9	
	Train	Test	Train	Test	Train	Test
Dreamer	250.2 \pm 9.6	3.0 \pm 2.2	237.4 \pm 14.9	28.9 \pm 14.6	168.7 \pm 96.2	157.2 \pm 188.4
TAD	951.9 \pm 3.3	876.9 \pm 51.1	841.9 \pm 154.9	546.1 \pm 291.6	777.7 \pm 170.1	716.8 \pm 136.5

Table 7: Average cumulative reward (mean \pm one std) over different sparse rates of the best policy trained by Dreamer and TAD in Cheetah.Speed. For each sparse rate, we train agents in the train tasks and evaluate them in both train and test environments. Numbers greater than 95 percent of the best performance for each environment are **bold**.

reward function sparse, i.e., the output reward is the same as Cheetah.speed every n timesteps (in step $n - 1, 2n - 1, \dots$) and 0 otherwise, of which the sparse rate (SR) is $(n - 1)/n$. We supplement experiments to evaluate the performance of Dreamer and TAD with $n = 5$ (SR=0.8) and $n = 10$ (SR=0.9). As shown in Table 7, with the increasing of SR, although the performance of TAD decrease since inferring task context from sparse reward is extremely difficult, TAD still shows strong performance in train tasks and generalizes well to unseen test tasks.

F Ethics Issues and Border Impact

Designing agents that can generalize to unseen tasks is a major concern in reinforcement learning. This work focuses on task generalization in reinforcement learning and proposes a novel algorithm Reward Informed Dreamer. One of the potential negative impacts is that algorithms using deep neural networks, which lack interoperability and theoretical guarantee. If we hope to apply them in real-world applications, they may face security and robustness issues, and a possible way is to develop more explainable methods. There are no serious ethical issues as this is basic research. We hope our work can inspire more research on designing agents with stronger generalization abilities.

References

- [Chen *et al.*, 2021] Chang Chen, Jaesik Yoon, Yi-Fu Wu, and Sungjin Ahn. Transdreamer: Reinforcement learning with transformer world models. In *Deep RL Workshop NeurIPS 2021*, 2021.
- [Chung *et al.*, 2014] Junyoung Chung, Caglar Gulcehre, KyungHyun Cho, and Yoshua Bengio. Empirical evaluation of gated recurrent neural networks on sequence modeling. *arXiv preprint arXiv:1412.3555*, 2014.
- [Clavera *et al.*, 2018] Ignasi Clavera, Jonas Rothfuss, John Schulman, Yasuhiro Fujita, Tamim Asfour, and Pieter Abbeel. Model-based reinforcement learning via meta-policy optimization. In *Conference on Robot Learning*, pages 617–629. PMLR, 2018.
- [Cobbe *et al.*, 2019] Karl Cobbe, Oleg Klimov, Chris Hesse, Taehoon Kim, and John Schulman. Quantifying generalization in reinforcement learning. In *International Conference on Machine Learning*, pages 1282–1289. PMLR, 2019.
- [Deng *et al.*, 2022] Fei Deng, Ingook Jang, and Sungjin Ahn. Dreamerpro: Reconstruction-free model-based reinforcement learning with prototypical representations. In *International Conference on Machine Learning*, pages 4956–4975. PMLR, 2022.
- [Duan *et al.*, 2016] Yan Duan, John Schulman, Xi Chen, Peter L Bartlett, Ilya Sutskever, and Pieter Abbeel. RL²: Fast reinforcement learning via slow reinforcement learning. *arXiv preprint arXiv:1611.02779*, 2016.
- [Finn *et al.*, 2017] Chelsea Finn, Pieter Abbeel, and Sergey Levine. Model-agnostic meta-learning for fast adaptation of deep networks. In *International conference on machine learning*, pages 1126–1135. PMLR, 2017.
- [Fu *et al.*, 2021] Xiang Fu, Ge Yang, Pulkit Agrawal, and Tommi Jaakkola. Learning task informed abstractions. In *International Conference on Machine Learning*, pages 3480–3491. PMLR, 2021.
- [Ghosh *et al.*, 2021] Dibya Ghosh, Jad Rahme, Aviral Kumar, Amy Zhang, Ryan P Adams, and Sergey Levine. Why

- generalization in rl is difficult: Epistemic pomdps and implicit partial observability. *Advances in Neural Information Processing Systems*, 34:25502–25515, 2021.
- [Ha and Schmidhuber, 2018] David Ha and Jürgen Schmidhuber. World models. *arXiv preprint arXiv:1803.10122*, 2018.
- [Hafner *et al.*, 2019a] Danijar Hafner, Timothy Lillicrap, Jimmy Ba, and Mohammad Norouzi. Dream to control: Learning behaviors by latent imagination. In *International Conference on Learning Representations*, 2019.
- [Hafner *et al.*, 2019b] Danijar Hafner, Timothy Lillicrap, Ian Fischer, Ruben Villegas, David Ha, Honglak Lee, and James Davidson. Learning latent dynamics for planning from pixels. In *International conference on machine learning*, pages 2555–2565. PMLR, 2019.
- [Hafner *et al.*, 2020] Danijar Hafner, Timothy P Lillicrap, Mohammad Norouzi, and Jimmy Ba. Mastering atari with discrete world models. In *International Conference on Learning Representations*, 2020.
- [Hafner *et al.*, 2023] Danijar Hafner, Jurgis Pasukonis, Jimmy Ba, and Timothy Lillicrap. Mastering diverse domains through world models. *arXiv preprint arXiv:2301.04104*, 2023.
- [Hansen and Wang, 2021] Nicklas Hansen and Xiaolong Wang. Generalization in reinforcement learning by soft data augmentation. In *2021 IEEE International Conference on Robotics and Automation (ICRA)*, pages 13611–13617. IEEE, 2021.
- [Janner *et al.*, 2019] Michael Janner, Justin Fu, Marvin Zhang, and Sergey Levine. When to trust your model: Model-based policy optimization. *Advances in neural information processing systems*, 32, 2019.
- [Kakade and Langford, 2002] Sham Kakade and John Langford. Approximately optimal approximate reinforcement learning. In *In Proc. 19th International Conference on Machine Learning (ICML)*. Citeseer, 2002.
- [Laskin *et al.*, 2020] Michael Laskin, Aravind Srinivas, and Pieter Abbeel. Curl: Contrastive unsupervised representations for reinforcement learning. In *International Conference on Machine Learning*, pages 5639–5650. PMLR, 2020.
- [Lee *et al.*, 2019] Kimin Lee, Kibok Lee, Jinwoo Shin, and Honglak Lee. Network randomization: A simple technique for generalization in deep reinforcement learning. In *International Conference on Learning Representations*, 2019.
- [Lee *et al.*, 2020] Kimin Lee, Younggyo Seo, Seunghyun Lee, Honglak Lee, and Jinwoo Shin. Context-aware dynamics model for generalization in model-based reinforcement learning. In *International Conference on Machine Learning*, pages 5757–5766. PMLR, 2020.
- [Lee *et al.*, 2022] Kuang-Huei Lee, Ofir Nachum, Mengjiao Sherry Yang, Lisa Lee, Daniel Freeman, Sergio Guadarrama, Ian Fischer, Winnie Xu, Eric Jang, Henryk Michalewski, et al. Multi-game decision transformers. *Advances in Neural Information Processing Systems*, 35:27921–27936, 2022.
- [Mnih *et al.*, 2016] Volodymyr Mnih, Adria Puigdomenech Badia, Mehdi Mirza, Alex Graves, Timothy Lillicrap, Tim Harley, David Silver, and Koray Kavukcuoglu. Asynchronous methods for deep reinforcement learning. In *International conference on machine learning (ICML)*, pages 1928–1937. PMLR, 2016.
- [Mu *et al.*, 2022] Yao Mark Mu, Shoufa Chen, Mingyu Ding, Jianyu Chen, Runjian Chen, and Ping Luo. Ctrlformer: Learning transferable state representation for visual control via transformer. In *International Conference on Machine Learning*, pages 16043–16061. PMLR, 2022.
- [Nagabandi *et al.*, 2018] Anusha Nagabandi, Ignasi Clavera, Simin Liu, Ronald S Fearing, Pieter Abbeel, Sergey Levine, and Chelsea Finn. Learning to adapt in dynamic, real-world environments through meta-reinforcement learning. In *International Conference on Learning Representations*, 2018.
- [Nguyen *et al.*, 2021] Tung D Nguyen, Rui Shu, Tuan Pham, Hung Bui, and Stefano Ermon. Temporal predictive coding for model-based planning in latent space. In *International Conference on Machine Learning*, pages 8130–8139. PMLR, 2021.
- [Raileanu and Fergus, 2021] Roberta Raileanu and Rob Fergus. Decoupling value and policy for generalization in reinforcement learning. In *International Conference on Machine Learning*, pages 8787–8798. PMLR, 2021.
- [Raileanu *et al.*, 2021] Roberta Raileanu, Maxwell Goldstein, Denis Yarats, Ilya Kostrikov, and Rob Fergus. Automatic data augmentation for generalization in reinforcement learning. *Advances in Neural Information Processing Systems*, 34:5402–5415, 2021.
- [Rakelly *et al.*, 2019] Kate Rakelly, Aurick Zhou, Chelsea Finn, Sergey Levine, and Deirdre Quillen. Efficient off-policy meta-reinforcement learning via probabilistic context variables. In *International conference on machine learning*, pages 5331–5340. PMLR, 2019.
- [Robine *et al.*, 2023] Jan Robine, Marc Höftmann, Tobias Uelwer, and Stefan Harmeling. Transformer-based world models are happy with 100k interactions. *arXiv preprint arXiv:2303.07109*, 2023.
- [Schulman *et al.*, 2015] John Schulman, Philipp Moritz, Sergey Levine, Michael Jordan, and Pieter Abbeel. High-dimensional continuous control using generalized advantage estimation. *arXiv preprint arXiv:1506.02438*, 2015.
- [Sekar *et al.*, 2020] Ramanan Sekar, Oleh Rybkin, Kostas Daniilidis, Pieter Abbeel, Danijar Hafner, and Deepak Pathak. Planning to explore via self-supervised world models. In *International Conference on Machine Learning*, pages 8583–8592. PMLR, 2020.
- [Seo *et al.*, 2022] Younggyo Seo, Kimin Lee, Stephen L James, and Pieter Abbeel. Reinforcement learning with

- action-free pre-training from videos. In *International Conference on Machine Learning*, pages 19561–19579. PMLR, 2022.
- [Sodhani *et al.*, 2021] Shagun Sodhani, Amy Zhang, and Joelle Pineau. Multi-task reinforcement learning with context-based representations. In *International Conference on Machine Learning*, pages 9767–9779. PMLR, 2021.
- [Song *et al.*, 2019] Xingyou Song, Yiding Jiang, Stephen Tu, Yilun Du, and Behnam Neyshabur. Observational overfitting in reinforcement learning. In *International Conference on Learning Representations*, 2019.
- [Sutton and Barto, 2018] Richard S Sutton and Andrew G Barto. *Reinforcement learning: An introduction*. MIT press, 2018.
- [Tassa *et al.*, 2018] Yuval Tassa, Yotam Doron, Alistair Muldal, Tom Erez, Yazhe Li, Diego de Las Casas, David Budden, Abbas Abdolmaleki, Josh Merel, Andrew LeFrancq, et al. Deepmind control suite. *arXiv preprint arXiv:1801.00690*, 2018.
- [Todorov *et al.*, 2012] Emanuel Todorov, Tom Erez, and Yuval Tassa. Mujoco: A physics engine for model-based control. In *2012 IEEE/RSJ international conference on intelligent robots and systems*, pages 5026–5033. IEEE, 2012.
- [Touati and Ollivier, 2021] Ahmed Touati and Yann Ollivier. Learning one representation to optimize all rewards. *Advances in Neural Information Processing Systems*, 34:13–23, 2021.
- [Touati *et al.*, 2022] Ahmed Touati, Jérémy Rapin, and Yann Ollivier. Does zero-shot reinforcement learning exist? In *The Eleventh International Conference on Learning Representations*, 2022.
- [Van der Maaten and Hinton, 2008] Laurens Van der Maaten and Geoffrey Hinton. Visualizing data using t-sne. *Journal of machine learning research*, 9(11), 2008.
- [Vaswani *et al.*, 2017] Ashish Vaswani, Noam Shazeer, Niki Parmar, Jakob Uszkoreit, Llion Jones, Aidan N Gomez, Łukasz Kaiser, and Illia Polosukhin. Attention is all you need. *Advances in neural information processing systems*, 30, 2017.
- [Wang *et al.*, 2020] Kaixin Wang, Bingyi Kang, Jie Shao, and Jiashi Feng. Improving generalization in reinforcement learning with mixture regularization. *Advances in Neural Information Processing Systems*, 33:7968–7978, 2020.
- [Wang *et al.*, 2022] Tongzhou Wang, Simon Du, Antonio Torralba, Phillip Isola, Amy Zhang, and Yuandong Tian. Denoised mdps: Learning world models better than the world itself. In *International Conference on Machine Learning*, pages 22591–22612. PMLR, 2022.
- [Xu *et al.*, 2022] Yingchen Xu, Jack Parker-Holder, Aldo Pacchiano, Philip J Ball, Oleh Rybkin, Stephen J Roberts, Tim Rocktäschel, and Edward Grefenstette. Learning general world models in a handful of reward-free deployments. *arXiv preprint arXiv:2210.12719*, 2022.
- [Yang *et al.*, 2020] Ruihan Yang, Huazhe Xu, Yi Wu, and Xiaolong Wang. Multi-task reinforcement learning with soft modularization. *Advances in Neural Information Processing Systems*, 33:4767–4777, 2020.
- [Yarats *et al.*, 2021] Denis Yarats, Amy Zhang, Ilya Kostrikov, Brandon Amos, Joelle Pineau, and Rob Fergus. Improving sample efficiency in model-free reinforcement learning from images. In *Proceedings of the AAAI Conference on Artificial Intelligence*, volume 35, pages 10674–10681, 2021.
- [Ying *et al.*, 2022] Chengyang Ying, Xinning Zhou, Hang Su, Dong Yan, Ning Chen, and Jun Zhu. Towards safe reinforcement learning via constraining conditional value-at-risk. *arXiv preprint arXiv:2206.04436*, 2022.
- [Young *et al.*, 2022] Kenny Young, Aditya Ramesh, Louis Kirsch, and Jürgen Schmidhuber. The benefits of model-based generalization in reinforcement learning. *arXiv preprint arXiv:2211.02222*, 2022.
- [Zhao *et al.*, 2021] Zihao Zhao, Anusha Nagabandi, Kate Rakelly, Chelsea Finn, and Sergey Levine. Meld: Meta-reinforcement learning from images via latent state models. In *Conference on Robot Learning*, pages 1246–1261. PMLR, 2021.
- [Zintgraf *et al.*, 2019] Luisa Zintgraf, Kyriacos Shiarlis, Maximilian Igl, Sebastian Schulze, Yarın Gal, Katja Hofmann, and Shimon Whiteson. Varibad: A very good method for bayes-adaptive deep rl via meta-learning. In *International Conference on Learning Representations*, 2019.